ABSTRACT

Title of Dissertation: Application of Chaotic Synchronization

and Controlling Chaos

to Communications

Vasily Dronov, Doctor of Philosophy, 2005

Dissertation directed by: Professor Edward Ott
                           Department of Electrical and Computer Engineering

This thesis addresses two important issues that are applicable to chaotic communication systems: synchronization of chaos and controlling chaos. Synchronization of chaos is a naturally occurring phenomenon where one chaotic dynamical system mimics dynamical behavior of another chaotic system. This phenomenon can be used in chaotic communication system as a mechanism for information decoding whereas controlling chaos can be used to encode information into the dynamics of the system. Apart from this particular application, the phenomenon of chaotic synchronization is a popular topic of research, in general, and has attracted much attention within the scientific community. Controlling chaos is another potential engineering application. A unique property of controlling chaos is the ability to cause large long-term impact on the dynamics using arbitrarily small perturbations.

This thesis is broken up into three chapters. The first chapter contains a brief introduction to the areas of research of the thesis work, as well as the summaries the work itself. The second chapter is dedicated to the study of a particular situation of chaotic synchronization which leads to a novel structure of the basin of attraction. This chapter also develops theoretical scalings applicable to these systems and compares results of our numerical simulations on three different chaotic systems (two discrete maps and one continuous flow) with theoretical results.

The third chapter consists or two logically connected parts (as both of them study chaotic dynamics of systems that can be modeled with delayed differential equations). The first and the main part presents a study of a chaotically behaving traveling wave tube, or TWT, with the objective of improving efficiency of satellite communication systems. In this work we go through an almost complete design cycle, where, given an objective, we begin with developing a nonlinear model for a generic TWT; we then study numerically the dynamics of the proposed model; we find conditions where chaotic behavior occurs (we argue that TWT in chaotic mode could be more power efficient); then we use the idea of controlling chaos for information encoding; we support the concept with numerical simulations; and finally analyze the performance of the proposed chaotic communication system. The second part of this chapter describes an experiment with a pair of electronic circuits modeling the well-known Mackey-Glass equation. Despite the simplicity of the circuits, they represent a powerful experimental tool, as they are capable of exhibiting various types of dynamic behavior (fixed point, limit cycle, chaos including high-dimensional chaos with Lyapunov dimension >10). A simple experiment where human voice was encoded into chaotic sig-

nal had been conducted which showed a possibility of engineering application of chaos to secure communications.

Application of Chaotic Synchronization

and Controlling Chaos

to Communications

by

Vasily Dronov

Dissertation submitted to the Faculty of the Graduate School of the
University of Maryland, College Park in partial fulfillment
of the requirements for the degree of
Doctor of Philosophy
2005

Advisory Committee:

      Professor Edward Ott, Chairman/Advisor
      Professor Thomas M. Antonsen Jr., Co-Advisor
      Professor Rajarshi Roy, Co-Advisor
      Professor P. S. Krishnaprasad
      Professor Brian Hunt (Dean's Representative)

DEDICATION

Dedicated to my mother, Olga Roppe

my late father, Victor Dronov

and my wife, Sylvia Florez

for the support and inspiration they have provided.

ACKNOWLEDGEMENTS

While working on my research on the way to my Doctoral degree, I had the great fortune to meet and collaborate with many great people. First and foremost, I would like to acknowledge and thank my advisor, Prof. Edward Ott, for his invaluable advice, guidance, and patience. I would also like to thank Prof. Thomas M. Antonsen, Jr. and Prof. Rajarshi Roy for their personal attention and guidance. These three people have made a great contribution towards sharpening my ability to solve scientific problems by careful and complete examination and evaluation of the nature of the phenomena in question. I would also like to thank Pedro Safier and Baruch Levush at the Naval Research Lab for their guidance and valuable advice.

I also have benefited enormously from valuable discussions with my fellow students in the UMD Chaos group. In this regard I would like to mention Juan Restrepo, Matt Hendrey, David Sweet, Mitrajit Dutta, Mike Oczkovsky, Alexey Zimin and others.

TABLE OF CONTENTS

LIST OF TABLES

LIST OF FIGURES

Chapter 1

Introduction

Synchronization of chaos and controlling chaos are two subjects that are key to the use of chaos as a mean of information transport. Synchronization of dynamical systems is an ability of one system to mimic dynamical behavior of another system in a precise manner. The phenomenon of chaotic synchronization was described for the first time by Afraimovich et al. [1] and later applied to secure communications by Pecora and Carroll and [2]. Suppose that the dynamics of two systems are each described in terms of a set of, say, N state variables; Then, if viewed as parts or subsystems of a bigger system, a higher dimentional state space with dimention $2N$ can be introduced to simultaneously describe the dynamical behavior of both subsystems. If the dynamics of both subsystems are independent, all $2N$ state variables will be required to describe dynamical behavior of the overall system. If, however, the subsystems are either partially or fully synchronized, the resulting dynamics of the bigger system will be limited to a lower dimentional subspace which we call a "synchronization manifold", or in more general terms, an "invariant manifold". In the case where the synchronization manifold is transversely attractive, the chaotic systems will always synchronize. In general, however, the presence of an invariant manifold does not
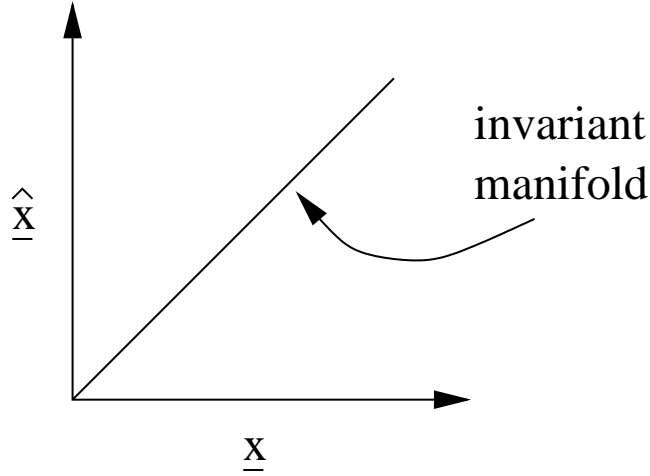
Figure 1.1: Graphical representation of invariant manifold for a general example described by Eq.(1.1)

guarantee synchronization. Synchronization persists for initial conditions lying in the invariant manifold (see Fig.1.1). However, an initial condition not in the invariant manifold may or may not lead to chaotic synchronization. The dynamical behavior of coupled chaotic systems, therefore, will be influenced by the stability properties of the chaotic dynamics in the invariant manifold. Therefore, studying properties of invariant manifolds is useful in terms of characterizing chaos-based communication systems where synchronization of chaos is being used as a means of information transmission-decoding process. An example of a system that has an invariant manifold is the following:

$$\frac{d\underline{x}}{dt} = \underline{F}(\underline{x}), \quad \frac{d\underline{\hat{x}}}{dt} = \underline{F}(\underline{\hat{x}}) + \underline{\underline{K}}(\underline{x} - \underline{\hat{x}}) \tag{1.1}$$

If $\underline{x} = \underline{\hat{x}}$ initially, then the coupling term on the right side of the $\frac{d\underline{\hat{x}}}{dt}$ equation is identically zero, and $\underline{x} = \underline{\hat{x}}$ is true for all time.

Examples show that dynamical systems that exhibit chaotic dynamics on an
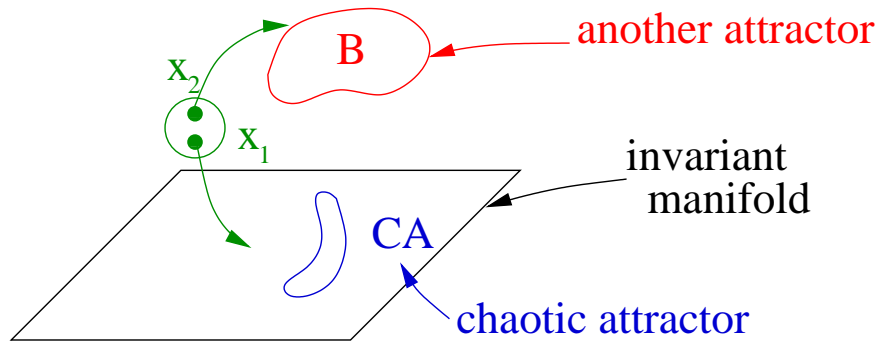
Figure 1.2: Situation that leads to riddling
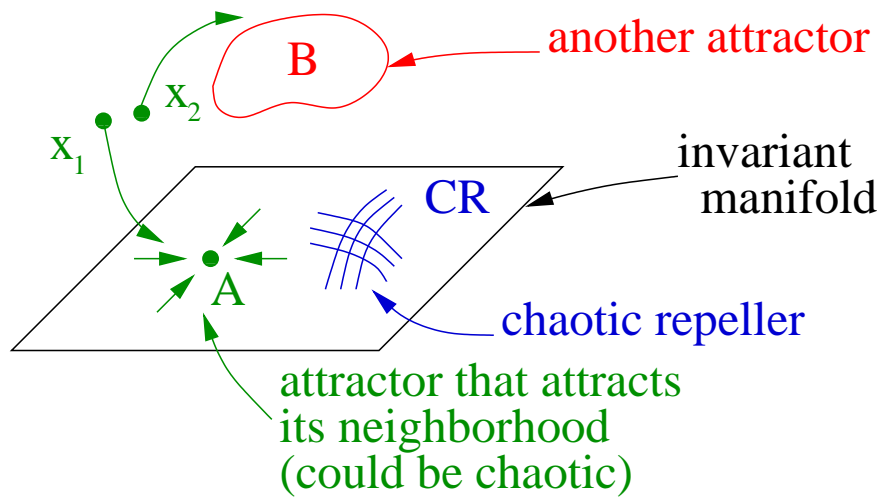
Figure 1.3: Situation that leads to "stalactites"

invariant manifold embedded in their state space may yield novel dynamical behaviors. One such situation is the case where the chaotic set in the invariant manifold is attracting on average but has within it invariant subsets that are repelling transverse to the invariant manifold. In appropriate circumstances this leads to so called "riddling" of the basin of attraction (see Fig.1.2, Ref. [3,4]). In Chapter 2 of this thesis we consider a related, but different, situation where there is both a nonattracting chaotic set and an attractor which is "absolutely attracting" in the invariant manifold. Here by "absolutely attracting" we mean that the attractor is attracting for points in the invariant manifold and *all* invariant sets within the attractor are transversely attracting (e.g., the absolutely attracting attractor might be a stable periodic orbit). Thus in the full phase space there is an open neighborhood of the absolutely attracting attractor that is part of its basin of attraction. It is found that in such a case the basin boundary of the attractor in the invariant manifold may be characterized by thin stalactite like structure emanating from the nonattracting chaotic set in the invariant manifold (see Fig. 1.3). We employ a Fokker-Planck type model which shows that, near the invariant manifold, the state space measure (volume) not in the basin of the attractor on the invariant manifold scales as a power law of the displacement from the invariant manifold. The solution to the Fokker-Planck model for the power law exponent is in a good agreement with numerical tests.

Also note that dynamical systems that exhibit chaotic dynamics on an invariant manifold embedded in their state space can also be of great interest in situations other than communicating with chaos. To emphasize the universality of this work, it is worth mentioning a recent study [5] which addresses a common predator-pray model yielding a very similar situation, where the basin of

the attractor can be characterized by the stalactites-like structure described in Chapter 2.

Chapter 3 of this thesis is mainly devoted to the control of chaotic behavior in a traveling wave tube (TWT). Traveling wave tubes [6–8] are microwave-range, high-power amplifiers commonly used on communication satellites. We model TWT dynamics using a delay differential equation. In other situation where related delay models are used, similar behavioral patterns are observed. We believe, therefore, that results of this study are applicable in a variety of situations where one is attempting to build a chaotic communication system in which chaotic oscillations are utilized for information transmission and where a physical mechanism introduces signal propagation delay in the transmitter signal generator. We will refer to the class of such systems as time-delayed feedback dynamical systems.

Time-delayed feedback dynamical systems have recently received much attention [9–15, 17]. Examples of such systems are: ring lasers [11, 14, 17], where light travels inside a closed loop which contains a nonlinear optical amplifier; another example is a Mackey-Glass equation [9, 12, 13] which represents a mathematical model for haematologic disorders (we conducted an electronic experimental implementation of this system; see Sec.3.2); yet another example is our nonlinear model of a traveling tube amplifier (TWT) [15, 16, 18–22] (see Sec.3.1).

A general form for a class of such dynamical systems is

$$\dot{x}(t) + x(t) = f(p, x(t - \tau)), \tag{1.2}$$

where x is the state variable of the system and p is a bifurcation parameter. (Note that x can be complex in general. In the case of the TWT model, an important factor determining qualitative behavior is than the ratio between the delay time τ and the decay time of $x(t)$ [the latter is normalized to one in Eq.(1.2)].

Despite the variety of nonlinearities which can arise in such systems, many such systems share similar properties and exhibit similar behavior. One common observation for the class of dynamical systems described by Eq.(1.2) is the presence of a low-dimensional chaotic attractor for relatively small delays τ, which transforms into a more complicated (i.e., higher dimensional) chaotic attractor for higher values of τ and eventually becomes very high-dimensional ("very" means Lyapunov dimension [see Ref. [23]] $D_L \geq 10$) for relatively large values of τ (see Fig.(1.4)).

Three possible applications of time-delayed feedback dynamical systems to chaotic communications are:

1. Implementation of high-speed dynamic memory in systems similar to a ring laser [14]. Numerous self-sustaining modes can be excited in such a system, and therefore short bit sequences can be written, stored and erased at a very high speed. This application holds promise for a storage device for ultra-high speed data, although it might be difficult to use such a memory element in practice. Aida and Davis built and demonstrated such a device [14].

2. Controlling the symbolic dynamics of a chaotic transmitting system for digital communications [24–27]. Our research in Chapter 3 reports on developing a nonlinear model for a TWT operating in the saturation regime [15,16]. Our theoretical model for the TWT accounts for power saturation, phase nonlinearity, and reflections from the mismatched load. This model exhibited a rich variety of dynamical behavior. We have found that for certain sets of parameters of the model we can observe a low-dimensional chaotic flow in a higher dimensional phase space. The symbolic dynamics of such flow can be controlled [25–27]. This approach was proven to work well with

6

our TWT model using computer simulations, although a real experiment has not been performed yet. We have studied both the first-order model as well as a more complex second-order model of TWT; both models yielded similar behavior. We have also analyzed performance of a chaotic TWT based communication system in noisy environment.

Reference [16] was dedicated to the time-domain modeling of an existing TWT. The objective was to study a combined effect of the saturation and reflections on the distortion of high-rate (100 Megasymbols/sec) QAM-modulated signal. The novelty of the time-domain model is that it allowed us to relate digital performance to the physical characteristics of the device.

3. Masking the information bearing signal with a chaotic signal [28–32]. In this scheme, message recovery is possible due to the synchronization phenomenon. An example showing experimental evidence of synchronization in time-delayed systems are recent studies of ring-laser systems [11, 17]. In these experiments, the dynamics of one laser was affected by binary digital information, which was then retrieved from the second nonlinear laser amplifier through use of a suitable detection scheme.

At the end of Chapter 3 we also include the descripton of the pair of electronic circuits which are a representation of the Mackey-Glass system. Using these circuits, we demonstrated the possibility of voice signal encoding and recovery using simple electronic time-delayed nonlinear feedback circuits. These circuits may also be used to conduct experimental study of chaotic multiplexing/demultiplexing [33, 34], as well as to characterize chaotic behavior of time-delayed feedback systems that have more than one delayed feedback.

Nonlinear time-delayed feedback loops describe a large class of physical systems. Therefore, good understanding of the dynamics of such systems will lead to better understanding of the underlying phenomena occuring in such systems, with the possibility of new engineering applications.
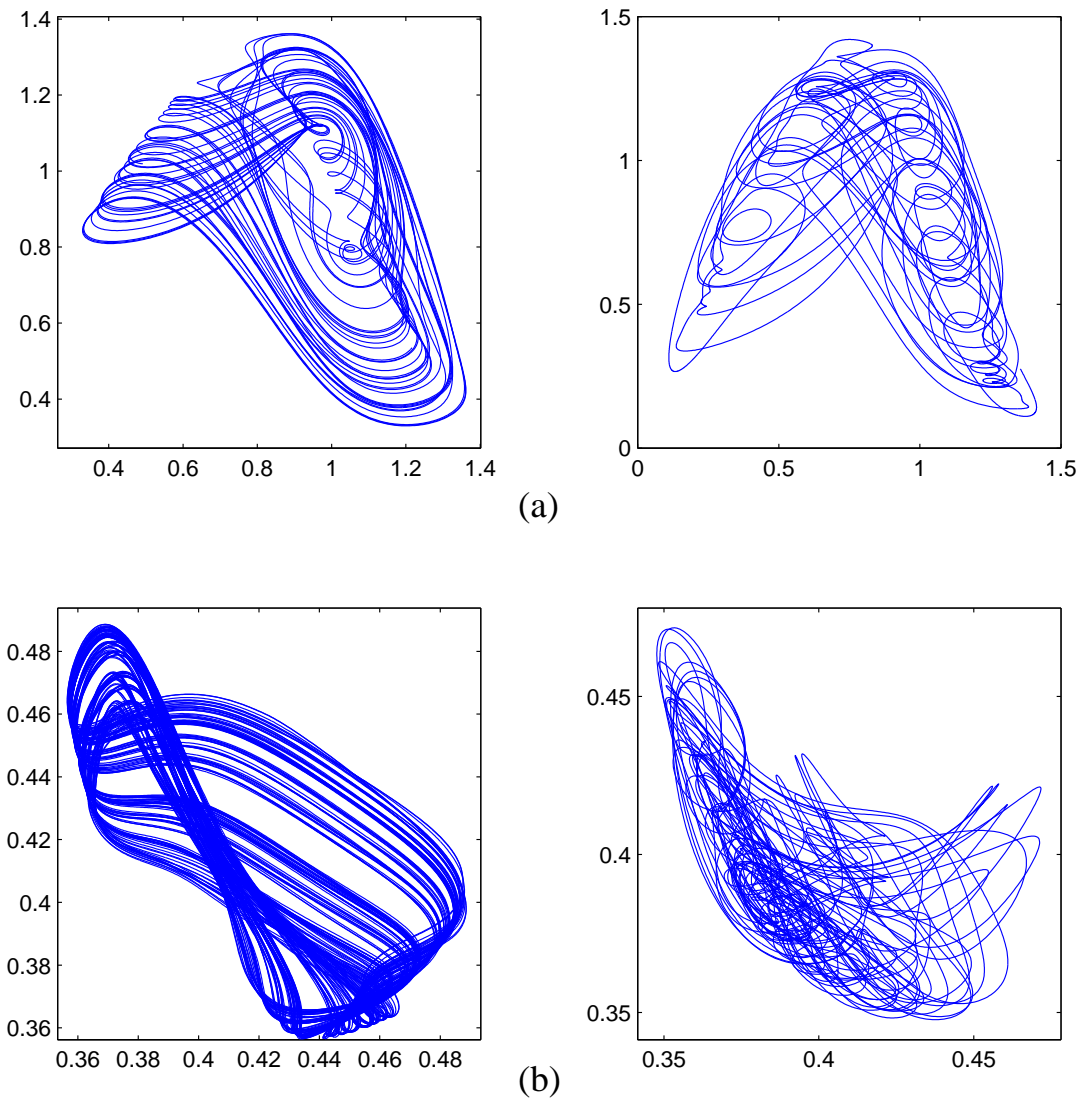
Figure 1.4: Similarity between dynamics of Mackey-Glass system (a) and the model of TWT (b). Both system exhibit low-dimensional behavior for $\tau \sim 1$ (on the left) and high-dimensional behavior for $\tau \gg 1$ (on the right).

Chapter 2

Stalactite Basin Structure of Dynamical Systems
with Transient Chaos in an Invariant Manifold

2.1   Introduction

[1] Recently, physically important examples of dynamical systems that have invariant manifolds embedded in their phase space have been studied, and some important dynamical consequences of this have been revealed. An important class of systems that have invariant manifolds are those that possess an appropriate symmetry. In this case any initial state that has the same symmetry as the system evolves to other states that also respect the symmetry of the system. The set of such symmetric initial states then forms a manifold that is invariant under the dynamics of the system. An example of an invariant manifold not accompanied by a symmetry of the dynamical system is the case of one-way coupling of two

---

[1]This chapter is a verbatim representation of the paper by V. Dronov and E. Ott, Stalactite Basin Structure of Dynamical Systems with Transient Chaos in an Invariant Manifold, *Chaos*, Volume 10, No. 2, June 2000

identical oscillators, for which the states where the oscillators are synchronized form an invariant manifold.

An invariant manifold (whether induced by symmetry or not) can also have the property that the dynamics restricted to this manifold is chaotic, i.e. initial states in the manifold can be attracted to some chaotic set A in the invariant manifold. Thus A is an attractor for initial conditions in the invariant manifold. Note, however, that A may or may not be an attractor for the full system. Here by an attractor for the full system we mean that the set A attracts a set of initial conditions of positive Lebesgue measure in the full phase space [35]. In what follows, if we say, without qualification, that A is an attractor, then we mean that it is an attractor for the full system.

Considering the case where A is an attractor, there are typical cases where there is a small set of points in any neighborhood of the invariant manifold, that move away from A as the dynamical system evolves. If the global dynamics of the system is such that these repelled orbits are attracted to a set other than A, then the basin of attraction of A is *riddled* [3,4]. That is, if r is any point in the basin of A, then, for every ν, no matter how small, there is a displacement $\delta, |\delta| < \nu$, such that the point $r + \delta$ is in the basin of another attractor, and the set of such points, $r + \delta, |\delta| < \nu$, has nonzero phase space volume (i.e., positive Lebesgue measure). This presents a basic obstruction to determinism in such systems: If one does an experiment by preparing an initial condition and observes that the resulting orbit goes to A, then no matter how great one's precision in preparing the initial condition, one can not be sure that an attempted repeat of the experiment will result in the same outcome.

The unusual properties of riddled basins have received much attention. Re-

cent work [36–39] has investigated the transition to chaotic attractors with riddled basins and the effect of noise and asymmetry on the dynamics of systems with riddled basins. To treat the transition to chaotic attractors with riddled basins, a simple analyzable diffusion model [36] was proposed and scaling relations consistent with numerical simulations were obtained [40].

The main question addressed in this paper is what happens if, instead of a chaotic attractor embedded in the invariant manifold, there is a chaotic repeller for the initial conditions in the invariant manifold. By a chaotic repeller we mean an invariant set on which the dynamics is chaotic, but which does not attract a positive Lebesgue measure set of initial conditions in the invariant manifold. Typically, such nonattracting chaotic sets manifest themselves as chaotic transients [41]. For the case we consider, an initial condition in the invariant manifold can experience a chaotic transient, after which it is attracted to a periodic orbit in the invariant manifold.

As we shall show, when a chaotic repeller is in the manifold, the basin of the periodic orbit attractor in the invariant manifold is no longer riddled, although it still has unusual properties.

This new situation is illustrated schematically in Fig.2.1, where we use a two-dimensional x-y representation. In this figure $y = 0$ represents the invariant manifold. The dot represents the non-chaotic attractor in the $y = 0$ invariant manifold, and the vertical tic marks represent the chaotic repeller in $y = 0$. From every point in the chaotic repeller there emanates a cusp-shaped region (a stalactite) of the basin of the attractor in $y \neq 0$. Only one of these cusp-shaped regions is shown in Fig.2.1, but we emphasize that such regions exist for all points in the chaotic repeller. Note that since the attractor (the dot in Fig.2.1)
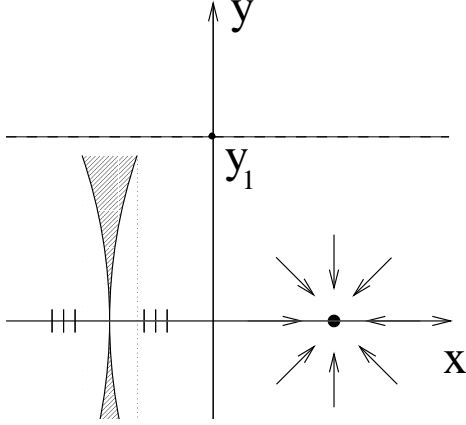
Figure 2.1: Schematic of the situation where there is a chaotic repeller (vertical tic marks) and a periodic orbit (solid dot) in the invariant manifold $(y = 0)$

attracts a neighborhood of itself, its basin is not riddled. Nevertheless, there is a remnant of the previously studied riddled behavior in the infinite number of cusps of the $y \neq 0$ attractor emanating from the invariant manifold $y = 0$. To characterize this situation we shall be interested in the scaling of the size of the $y \neq 0$ attractor's basin in the region near the invariant manifold $(y = 0)$. In particular, we will consider a horizontal line $y = y_1$ (see Fig.2.1) and ask what is the Lebesgue measure of x-values in this line that are attracted to the $y \neq 0$ attractor. We find that for y_1 small this measure, denoted $P_\infty(y_1)$, exhibits a power law scaling, $P_\infty(y) \sim y^\alpha$. To arrive at this result, following Ref. [38], we modify the diffusion model of Ref. [36] previously used for the riddled case to account for the new situation pictured in Fig.2.1, and we use it to derive results for the scaling exponent α. We claim that these results are universal in the sense that they are valid for the class of dynamical systems of the type considered above.

In order to check our scaling relations numerically we studied three dynamical

systems. The first two are represented by two-dimensional maps. In the first two-dimensional map case the dynamics in the invariant manifold is described by the well-known logistic map, and we will be interested in parameter values in the vicinity of a type one intermittency transition [42]. In the second two-dimensional map case the logistic map is replaced with a map [43] exhibiting type three intermittency [42]. The third example is a system of ordinary differential equations (a flow) which is a modification of a previously studied system [4] that describes the motion of a particle in a two-dimensional potential well. As before, we are interested in parameter values near an intermittency transition. Our predicted scaling relations were tested for all three numerical models and reasonably good agreement with the theory was observed.

In a recent paper Lai and Grebogi [44] consider the same situation that we consider here. A main claim in that paper is that the basin is of a mixed type with the property that, in the vicinity of the saddle, the basin is riddled, while, in the region of the attracting periodic orbit in the invariant manifold, the basin is solid (i.e. it consists of open volumes and is not riddled). Such a mixed basin cannot occur, and the basin cannot be riddled anywhere. In general, if a basin is open in any neighborhood $\mathcal{N}$ of the attractor, it must be open everywhere. A simple argument showing this is as follows. Say p is a point in the basin. Evolving p forward, it must eventually approach the attractor. Thus, at some finite time, the orbit from p must eventually enter $\mathcal{N}$, say at point p'. The point p' in $\mathcal{N}$ necessarily has an open neighborhood in the basin. Since p iterates to p' in a finite number of iterates, p must also have an open neighborhood in the basin. Hence, in contradiction to the claim of [44], the basin cannot be riddled anywhere. Lai and Grebogi [44] also attempt to obtain the scaling $P_\infty(y) \sim y^\alpha$.

However, they use a crude model for the chaotic transient; in particular, in their model all points in the chaotic transient phase abruptly leave the transient at a fixed time equal to the average transient lifetime. In fact, there is a continuous long-time exponential decay of orbits in the chaotic transient, and it is necessary to include this in the model to obtain the correct scaling and the correct exponent α.

2.2 The Model

Consider a smooth two-dimensional map of the form,

$$y_{n+1} = N(x_n, y_n, \epsilon), \tag{2.1}$$

$$x_{n+1} = M(x_n, r). \tag{2.2}$$

where ϵ and r are parameters. Suppose that $N(x, 0, \epsilon) = 0$ so that there is an invariant manifold at $y = 0$. We also assume that $N(\cdot)$ is such that if $|y_n| > y_c$ then all subsequent y iterates are also in $|y| > y_c$; in particular, the orbit never comes back close to the $y = 0$ plane. Thus there is another attractor (or attractors) in $|y| > y_c$. Without loss of generality we let $y_c = 1$.

Following Ref. [38] we refer to ϵ as a "normal" parameter since it affects the dynamics normal to the $y = 0$ invariant manifold, but has no influence on the dynamics in the $y = 0$ invariant manifold [the dynamics in $y = 0$ is governed by Eq.(2.2)]. Similarly [38], we refer to r as a "non-normal parameter".

Suppose that for some value of r, $M(x, r)$ has a chaotic attractor in x and ϵ is such that riddling occurs. In this case $y = 0$ is an attractor and its Lyapunov exponent which we denote $h_\perp$ [calculated by taking a differential y variation of Eq.(2.1)] is negative, $h_\perp < 0$. In the riddled case, in any neighborhood of the
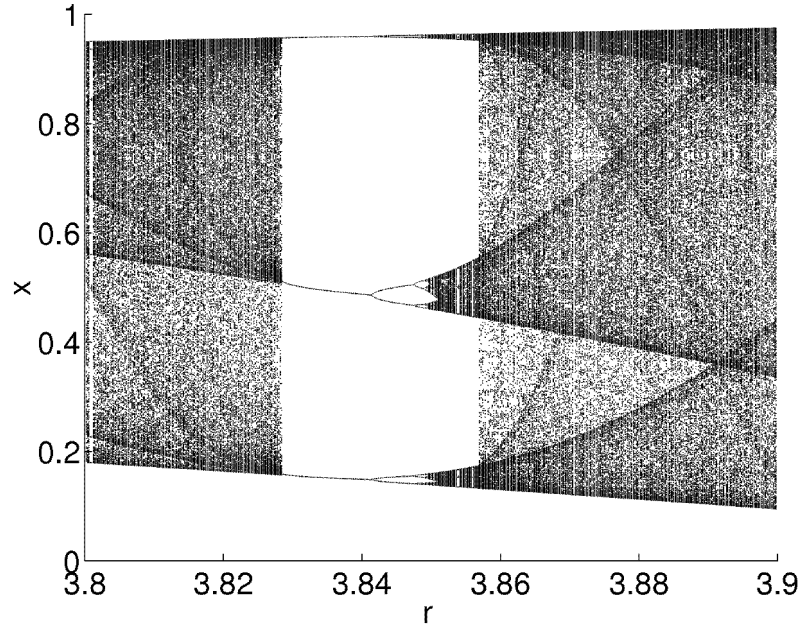
Figure 2.2: Period three window in the bifurcation diagram of the logistic map, $x_{n+1} = rx_n(1 - x_n)$.

$y = 0$ attractor there are initial conditions that stay in the neighborhood and go to the attractor, as well as other initial conditions that leave the neighborhood of $y = 0$, possibly moving to the $|y| > y_c$ attractor. What will happen if we change r in such a way that, for a typical initial condition x_0, $M(\cdot)$ generates a chaotic transient instead? (For example, if $M(\cdot)$ is the logistic map we can imagine a change of r such that we enter a periodic window, e.g., the period three window on the bifurcation diagram of the logistic map; see Fig.2.2.) This means that the original chaotic attractor in the invariant plane $y = 0$ does not exist any more and typical initial conditions in $y = 0$ eventually go to a nonchaotic attractor (e.g., a periodic orbit or a fixed point) as $n \to \infty$. There will still exist, however, an infinite nonattracting set of initial conditions $\{x_0^{inv}\}$ (representing the ghost of the former chaotic attractor) for which infinitely long chaotic orbits can be generated, and this set has zero Lebesgue measure in x.

Let $\langle h_\perp \rangle$ denote the y-Lyapunov exponent for a typical orbit on the $y = 0$ chaotic invariant set. Here by typical we mean with respect to the natural transient measure for the x map. In this case $\langle h_\perp \rangle$ is calculated by sprinkling N_0 initial conditions in $y = 0$, iterating them for n iterates, discarding those that are near the nonchaotic orbit (say, further than some appropriate distance l), calculating the $h_\perp$ exponents over the time interval 0 to n for each orbit not near the nonchaotic orbit at time n, and averaging these values. In the limit $N_0 \to \infty, n \to \infty$, this average is $\langle h_\perp \rangle$, the y-Lyapunov exponent, calculated with respect to the natural transient measure for the x map.

We show in the following that the basin of $|y| > y_c$ can be in the form of an infinite set of cusp-shaped regions emanating from the chaotic transient invariant set in the plane $y = 0$. We call these cusp-shaped regions stalactites. We show for our examples that the Lebesgue measure in x of these tongues in a $y = y_1$ cross section scales as y_1^α, where $\alpha > 1$. We also give a theory for determining α and obtain good agreement of the theory with numerical experiments. We note that stalactite boundaries can occur for both $\langle h_\perp \rangle > 0$ and $\langle h_\perp \rangle < 0$. For stalactites in the case $\langle h_\perp \rangle < 0$, however, it is also required that the chaotic saddle (although transversely attracting) have embedded periodic orbits with positive transverse Lyapunov exponents [44].

2.3   Diffusion approximation

Consider the map (2.1)-(2.2) and assume that there is a fixed point attractor $x = x_*$ for almost any initial condition in $y = 0$. Also assume that there is a chaotic transient set in $y = 0$. The transverse tangent map (evolving differential
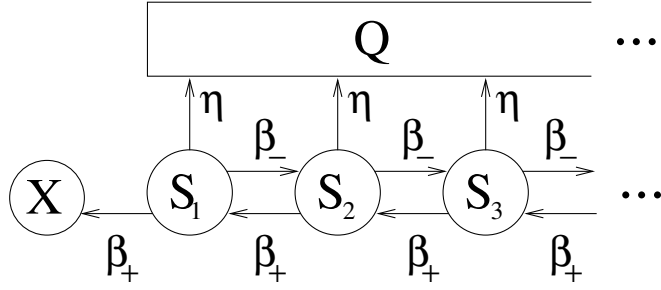
Figure 2.3: Markov chain.

y displacements from the invariant set $y = 0$) is

$$\delta y_{n+1} = N_y(0, x_n)\delta y_n,$$

where $N_y(0, x)$ denotes $\partial N/\partial y$ evaluated at $y = 0$. For an initial condition x_0 precisely on the chaotic transient set, the orbit x_n is typically chaotic. For x_1 on the nonchaotic attractor in $y = 0$ (i. e., $x = x_*$), we have $|N_y(0, x_n)| < 1$. Let $\delta z_n = -\ln|\delta y_n|$. Then the change in δz is given by $\delta z_{n+1} = \delta z_n + \Delta_n$, where $\Delta_n = -\ln|N_y(0, x_n)|$. During the chaotic transient x_n is chaotic, and hence Δ_n varies in a random manner. After the chaotic transient $\Delta_n \cong \ln|N_y(0, x_*)| < 0$. We follow Ref. [38] and model this situation as follows: Δ_n is taken to be of constant magnitude $|\Delta_n| = \Delta$ when the orbit is on the chaotic transient and fluctuations in Δ_n are modeled by random assignment of its sign $\Delta_n = \pm\Delta$, and we assume that the linearized dynamics is a good approximation to the actual dynamics for finite y in a neighborhood of $y = 0$. Thus on any given $\bar{y} \equiv \ln 1/|y|$ an iterate is represented by the step $\bar{y} \to \bar{y} \pm \Delta$, with $\bar{y} = +\infty$ ($\delta y = 0$) corresponding to $y = 0$. We consider a Markov chain model described by a semi-infinite chain of states S_i, $i = 0, 1, 2, \ldots$ (see Fig.2.3). We call the chain S_i the "chaotic chain". The model has three parameters β_+, β_- and η which represent the probabilities of the following transitions:

18

$\beta_+ : S_{i+1} \rightarrow S_i$ and $S_1 \rightarrow X$,

$\beta_-: S_i \rightarrow S_{i+1}$,

$\eta : S_i \rightarrow Q$.

The transition $S_{i+1} \rightarrow S_i$ $(S_i \rightarrow S_{i+1})$ represents a step in y away from (toward) the invariant surface $y = 0$, and in $\bar{y}$ it is represented by a step $\bar{y} \rightarrow \bar{y} - \Delta$ ($\bar{y} \rightarrow \bar{y}+\Delta$). X represents the condition $|y| > y_c$ for which the orbit goes to an attractor (or attractors) not in $y = 0$. After the transition $S_i \rightarrow Q$ $(S_1 \rightarrow X)$ the orbit is assumed to move uniformly in x (in y) toward the periodic attractor in $y = 0$ (the attractor in $|y| > y_c$). Once the chaotic chain is exited by transmission to Q or X, the chaotic transient is considered to be ended. We identify the transverse Lyapunov exponent with the random walk parameters via $\langle h_\perp \rangle = (\beta_+ - \beta_-)\Delta$. The question now becomes what is the probability of reaching the state X if starting at the state S_i? Our purpose in introducing this Markov model is to obtain a result for the scaling of the size of the $y \neq 0$ attractor basin in the region near $y = 0$. In particular, consider the horizontal line $y = y_1$. Different initial conditions $x = x_1$ on this line produce orbits, some of which go to the $y = 0$ attractor, and some of which go to the $y \neq 0$ attractor. We ask what fraction of the x-Lebesgue measure on $y = y_1$ goes to the $y \neq 0$ attractor. Denote this fraction $P_\infty(y_1)$. The above Markov model is relevant to this question in the following way. If we choose a point x_1 at random on the line $y = y_1$, then the probability that x_1 is in the basin of the $y \neq 0$ attractor is $P_\infty(y_1)$. Furthermore, as argued in Ref. [36], while the orbit is chaotic, the orbit generated for random x_1 can be regarded as random and as a stochastic process corresponding to a random walk on the S_i chain. However, the orbits following the chaotic transient can leave the S_i chain either by repulsion into the x region where the orbit moves

toward the nonchaotic orbit ($x = x_*$ on $y = 0$; i.e., $S_i \to Q$) or by repulsion in y into the region $|y| > y_c$ (i.e., $S_1 \to X$). Thus we can identify $P_\infty(y_1)$ with a random walker's probability $p(i)$ of reaching X starting at $i \sim \Delta^{-1} \ln |y_c/y_1|$. In particular, the large i scaling of $p(i)$,

$$p(i) \sim e^{-Ki}$$

and the small y_1 scaling of $P_\infty(y_1)$

$$P_\infty(y_1) \sim |y_1|^\alpha$$

are connected. Thus we now attempt to estimate K from the Markov model. Once this is accomplished, we will be in a position to use this to conjecture a general result for α, which we will compare with numerical experiments in Sec.4.

For the purposes of obtaining a solution for $p(i)$, we will apply the diffusion approximation, valid for $(\beta_+ - \beta_-)$ small [36], to the Markov model. Then the basic parameters of the diffusion model are the following:

(1) the average drift along the S_i chain per iterate, $v = \langle \delta \bar{y} \rangle$, where $\delta \bar{y}$ is the increment in $\bar{y}$ in one time step; by definition of the transverse Lyapunov exponent $v = -\langle h_\perp \rangle$;

(2) the diffusion per iterate, $D = \frac{1}{2} \langle (\delta \bar{y} - \langle \bar{y} \rangle)^2 \rangle$, where $\langle \cdots \rangle$ denotes an average over the initial random values of x_1;

(3) and an average lifetime of a typical chaotic transient τ.

Let $P(\bar{y}, \bar{y}_1, n)$ be the probability distribution function for $\bar{y}$ (given that x_1 is randomly chosen on the horizontal line segment $y = y_1$). Considering n to be approximated by a continuous variable (valid for $n \gg 1$), $P(\bar{y}, \bar{y}_1, n)$ obeys the following drift-diffusion equation:

$$\frac{\partial P}{\partial n} + v\frac{\partial P}{\partial \bar{y}} = -\frac{P}{\tau} + D\frac{\partial^2 P}{\partial \bar{y}^2}. \tag{2.3}$$

Since we imagine initial conditions all to start at $y = y_1$, we have

$$P(\bar{y}, \bar{y}_1, 0) = \delta(\bar{y} - \bar{y}_1), \bar{y}_1 > 0. \tag{2.4}$$

Since any orbit which crosses $y = y_c \equiv 1$ ($\bar{y} = 0$) is lost to the $y > 1$ attractor, we have

$$P(0, \bar{y}_1, n) = 0. \tag{2.5}$$

As discussed in [36], for this diffusion approximation to be valid we require two conditions:

- Many steps must be taken to reach $y = 1$ (corresponding to $\bar{y} = 0$), or $\bar{y}_1 \gg 1$.

- The drift on each iterate must be small, which means that $|\langle h_\perp \rangle| \ll 1$.

In order to solve Eq.(2.3) we will introduce the Laplace transform of $P(\bar{y}, \bar{y}_1, n)$ with respect to the continuous time variable n,

$$\bar{P}(\bar{y}, \bar{y}_1, s) = \int_0^\infty e^{-sn} P dn. \tag{2.6}$$

Eqs. (2.3)-(2.5) yield

$$D d^2 \bar{P}/d\bar{y}^2 - v d\bar{P}/d\bar{y} - (s + 1/\tau)\bar{P} = -\delta(\bar{y} - \bar{y}_1) \tag{2.7}$$

with the boundary condition $\bar{P}(0, \bar{y}_1, s) = 0$. Solving Eq.(2.7) is straightforward (see Appendix).

In Eq.(2.3), the term P/τ is the rate at which orbits leave the chaotic transient to move toward the attractor in $y = 0$. Thus the probability of going to the

attractor in the invariant manifold is

$$P_{y=0} = \frac{1}{\tau} \int_0^\infty \int_0^\infty P(\bar{y}, \bar{y}_1, n) d\bar{y} dn \tag{2.8}$$

and, therefore, the probability of getting attracted to the $y > 1$ attractor is

$$P_\infty = 1 - P_{y=0} = 1 - \frac{1}{\tau} \int_0^\infty \int_0^\infty P(\bar{y}, \bar{y}_1, n) d\bar{y} dn. \tag{2.9}$$

Performing the integration we finally get

$$P_\infty = y_1^\alpha, \; \alpha = \left[\sqrt{\langle h_\perp \rangle^2 + 4D/\tau} - \langle h_\perp \rangle \right]/2D. \tag{2.10}$$

The special case of small D $(D/\langle h_\perp \rangle^2 \tau \ll 1)$ yields,

$$\alpha \cong \begin{cases} (\langle h_\perp \rangle \tau)^{-1} & \text{for} \langle h_\perp \rangle > 0, \\[2mm] -\langle h_\perp \rangle/D & \text{for} \langle h_\perp \rangle < 0. \end{cases} \tag{2.11}$$

Note that, as expected, the result for $\langle h_\perp \rangle < 0$ and $\tau \to \infty$ agrees with the result for the exponent in the case of a riddled basin attractor, Ref. [36]. In the examples that follow $\langle h_\perp \rangle > 0$.

2.4 Numerical experiments

The universality of the phenomena addressed in this paper implies that very general results may be extracted from simple models that incorporate the essential features responsible for this phenomena. In this spirit we introduce three illustrative examples.

A. Example 1. The first example is the following two-dimensional map:

$$\begin{align} x_{n+1} &= M_1(x_n, r) = r x_n(1 - x_n) \tag{2.12} \\ y_{n+1} &= N_1(x_n, y_n, \epsilon, \epsilon') = \{1 + \epsilon - \epsilon'[1 - \cos(2\pi x_n)]\} y_n + y_n^3. \tag{2.13} \end{align}$$

22

This system has $N_1(x, 0, \epsilon, \epsilon') = 0$. Therefore, $y = 0$ is an invariant manifold for the map. The dynamics on this invariant manifold are generated by the logistic map and are independent of the parameters ϵ and ϵ'. Therefore, the parameters ϵ and ϵ' are normal parameters for the system (2.12)-(2.13). The value of r was chosen to be 3.837 which corresponds to the case of a period three attractor in the period-three window of the logistic map (see Fig.2.2). This implies that typical initial conditions in $0 < x_0 < 1$ and $y_0 = 0$ may generate chaotic transients. The average lifetime τ of such a transient depends on r and in our case is numerically determined to be $\tau = 21.41$. Note that if $y_n > [\frac{1}{3}(2\epsilon' - \epsilon)]^{1/2}$ then $y_{n+1} > y_n$ and the orbit evolves toward $y = \infty$, which we regard as the attractor not in $y = 0$. A numerical approximation to the basins of attraction is shown in Fig.2.4(a)-(b). To generate this figure we use a 5000×5000 grid of initial conditions, and we iterate each initial condition until it either reaches $y > [\frac{1}{3}(2\epsilon' - \epsilon)]^{1/2}$ (in which case we plot a black dot at the location of the initial condition) or else reaches a very small value of y, $y < 2 \times 10^{-5}$. In the later case we presume that, with high probability, the orbit will go to the $y = 0$ attractor. (This is justified by the scaling $P_\infty \sim y^\alpha$). We see in Fig.2.4(a)-(b) that there are many thin downward pointing black regions. From numerical examination of some of them by magnification of the horizontal scale we find that these thin black regions apparently extend down and touch the invariant set. They are stalactites referred to in Sec.1. The reason the stalactites appear in Fig.2.4(a)-(b) to terminate before reaching $y = 0$ is that they become so thin as y is decreased that they eventually fail to be resolved by our grid of initial conditions. In our simulations we took $\epsilon' = 0.8$ and varied the value of ϵ. For each value of ϵ we calculated $\langle h_\perp \rangle$, D, α_{th} and α_{exp}. The data is presented in the Table 2.1.
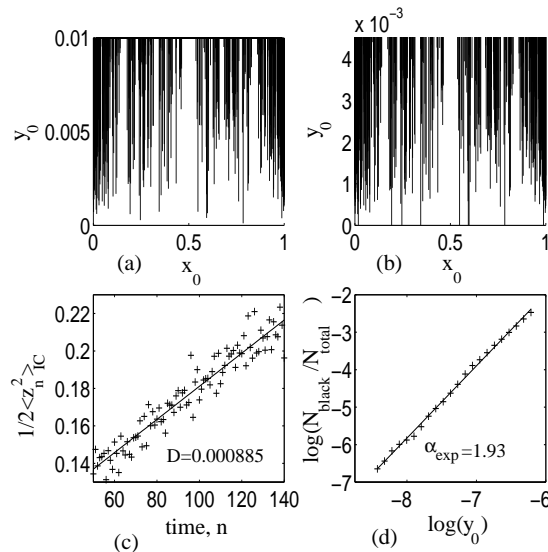
Figure 2.4: (a)-(b) shows basins of attraction for (2.12)-(2.13) for $\epsilon = 0.926$ and 0.928 respectively. To obtain (c) we uniformly sprinkle $L = 1.5 \times 10^6$ initial conditions in $y_0 = 0$, $0 < x_0 < 1$. We then iterate them 200 iterates and find that there are $l = 950$ orbits which still stay at a distance larger than 0.1 from the period three attractor. Then we plot $\frac{1}{2}\langle z_n^2 \rangle_{IC}$ versus n, where $\langle \ldots \rangle_{IC}$ denotes an average over the $l = 950$ orbits still not near the period three attractor. The value of D is then estimated as the slope of the straight line fit to the numerical data; (d) the fraction of initial conditions going to $y = \infty$ as a function of y. α_{exp} is obtained as the slope of the straight line fit to the data in a log-log scale. (c)-(d) correspond to the situation where $\epsilon = 0.926$.

To obtain the values of $\langle h_\perp \rangle$ for the chaotic transient set (second column of Table 2.1) we first uniformly sprinkle many initial conditions in $y_0 = 0$, $0 < x_0 < 1$. We then iterate these initial conditions M iterates. At time $M \gg 1$ most of the sprinkled orbits will be close to the attractor (say within a distance of 0.1). However, if the number of sprinkled orbits is large, there will still be orbits that are not near the attractor. We make the number of initial conditions sprinkled large enough so that there are still many initial conditions not near the attractor

ϵ	$\langle h_\perp \rangle$	D	α_{th}	α_{exp}
0.920	0.0164	0.000920	2.49	2.14
0.923	0.0200	0.000917	2.12	2.16
0.926	0.0233	0.000885	1.87	1.93
0.928	0.0256	0.000864	1.72	1.74

Table 2.1: Data for Example 1.

at time M. We then approximate $\langle h_\perp \rangle$ by

$$\langle h_\perp \rangle \cong \left\langle \frac{1}{M} \sum_{n=1}^{M} |\ln N_{1y}(x_n, 0)| \right\rangle_{IC},$$

where $N_{1y}(x, y) = \partial N_1 / \partial y$ and $\langle \ldots \rangle_{IC}$ denotes an average over those initial conditions whose orbits are not near the attractor in $y = 0$ at time M. The value of D (third column of Table 2.1) was obtained by noting that the quantity,

$$z_n = \sum_{m=1}^{n} (\ln |N_{1y}(x_m, 0)| - \langle h_\perp \rangle)$$

undergoes unbiased diffusion while the orbit is in the chaotic transient. Thus we plot $\frac{1}{2} \langle z_n^2 \rangle_{IC}$ versus n, and estimate D as the slope of a straight line fit to the data (see Fig.2.4(c) for an example of such a plot). The fourth column of Table 2.1, α_{th}, is then given by inserting $\langle h_\perp \rangle$ and D, as found above, into Eq.(2.10). The value of the experimental exponent α_{exp} (fifth column of Table 2.1) was obtained by estimating the fraction of "black" dots in the basin of attraction (those that lead to $y \to \infty$) as a function of y, and plotting this fraction as a function of y using a log-log scale. We find that, for sufficiently small y, such plots are, in accord with the predicted y^α dependence, well-fit by a straight line (see Fig.2.4(d) for example). The slope of such a fit gives α_{exp}. One can see from the Table 2.1 that α_{exp} agrees reasonably well with its predicted value α_{th}.
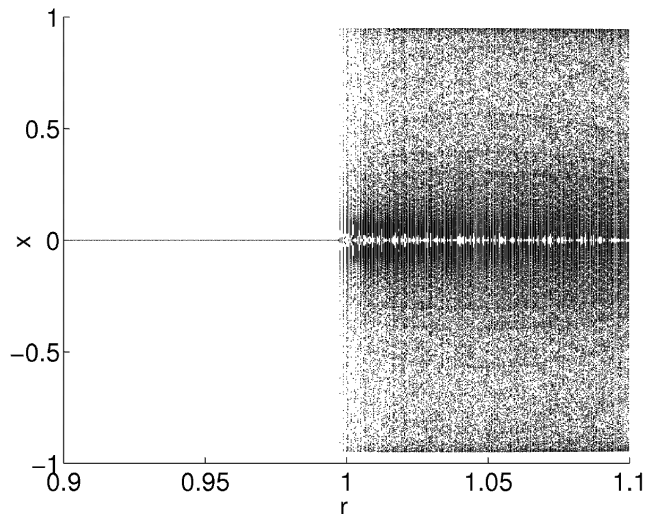
Figure 2.5: Bifurcation diagram for (2.14).

B. Example 2. We consider the two-dimensional map,

$$
x_{n+1} = M_2(x_n, r) = x_n[r(12.3 - 7r)x_n^4 - r(11.3 - 7r)x_n^2 + x_n^2 - r] \quad (2.14)
$$

$$
y_{n+1} = N_2(x_n, y_n, \epsilon, \epsilon') = \{1 + \epsilon - \epsilon'[1 + \cos(\pi x_n)]\}y_n + y_n^3. \quad (2.15)
$$

This system has the same general properties as in the map of the previous example. However, $M_2(x_n, r)$, the map in the invariant manifold, is an example [43] exhibiting type iii intermittency [42]. The bifurcation diagram for $M_2(\cdot)$ is shown in Fig.2.5. This map has a period one orbit at $x = 0$. As the parameter r increases through $r_c = 1$, this period one orbit becomes unstable, experiencing an inverse period doubling bifurcation. The map has a chaotic attractor for $r > 1$. The parameter r was taken to be equal to 0.95; $M_2(\cdot)$ is contracting at the fixed point $x = 0$ and repelling on a transient. For this value of r, we obtain $\tau = 28.0$. The basin of attraction is shown in Fig.2.6. The table below gives the values of $\langle h_\perp \rangle$, D, α_{th} and α_{exp} for $\epsilon' = 0.1$, and two different values of the other normal parameter ϵ:

C. Example 3. The third system we studied is a modification of a flow that

26
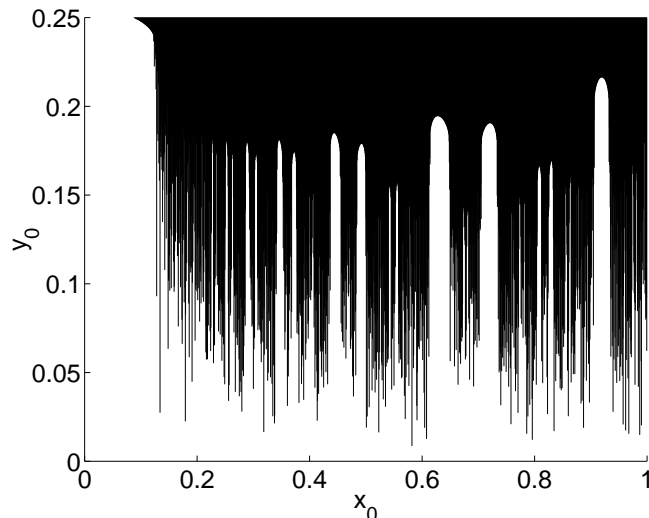
Figure 2.6: Basin of attraction for (2.14)-(2.15) obtained on 2000×2000 grid of initial conditions. $r = 0.95$, $\epsilon = 0.135$, $\epsilon' = 0.1$.

ϵ	$\langle h_\perp \rangle$	D	α_{th}	α_{exp}
0.150	0.005	0.011	1.59	1.62
0.155	0.010	0.011	1.40	1.42

Table 2.2: Data for Example 2.

describes the motion of a particle in a two dimensional (x, y) double potential well [4] $V(\mathbf{r}) = (1 - x^2)^2 + (x + \bar{x})y^2$. The particle is a subject to friction and time harmonic forcing,

$$d^2\mathbf{r}/dt^2 = -\gamma d\mathbf{r}/dt - \nabla V(\mathbf{r}) + f_0 \sin(\omega t)\hat{\mathbf{x}}. \tag{2.16}$$

Here $\hat{\mathbf{x}}$ is the unit vector in the x-direction and γ, f_0, ω and $\bar{x}$ are parameters. For appropriate $(\gamma, f_0, \omega, \bar{x})$ this system is known to exhibit a riddled basin [4]. The phase space of this problem is five-dimensional with coordinates x, dx/dt, y, dy/dt, and $\theta = (\omega t)$ mod 2π. From the symmetry of the potential the problem is invariant with respect to $y \to -y$, and, therefore, $y = dy/dt = 0$ specifies a three dimensional invariant hyperplane in the full five-dimensional phase space. The dynamics in this invariant hyperplane is obtained by setting y and dy/dt equal

27
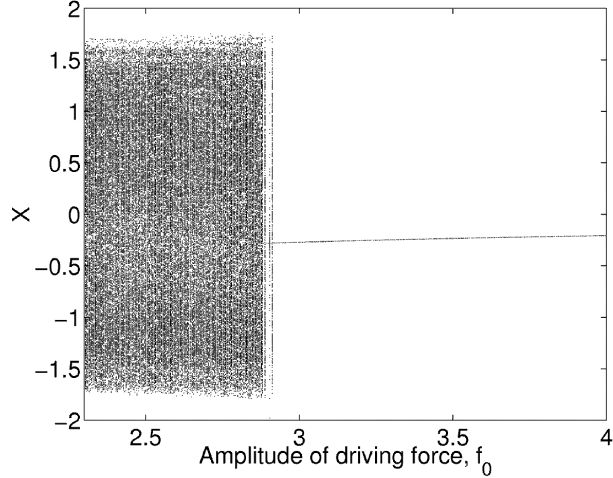
Figure 2.7: Bifurcation diagram for (2.17).

to zero in (2.16). This yields

$$d^2x/dt^2 + \gamma dx/dt - 4x(1 - x^2) = f_0 \sin(\omega t). \qquad (2.17)$$

We analyzed Eq.(2.16) in terms of a stroboscopic Poincare section corresponding to the period of the forcing, i.e. we consider the times $\omega t \bmod 2\pi = 0$. This lead to a four-dimensional discrete-time mapping.

In previous work using the model (2.16), the parameters γ, f_0 and ω were chosen so that (2.17) had a chaotic attractor. In this case, appropriate choice of the parameter $\bar{x}$ yields basin riddling for the $y = 0$ attractor. Here we consider a modification of (2.16) such that the dynamics in $y = 0$ is such that the attractor is periodic, but there is also a chaotic transient. In particular, we replace $\bar{x}$ by a time periodic quantity $\bar{x} = \bar{x}_0 + \bar{x}_1 \sin(\omega t - \phi)$ and set the parameters at $\bar{x}_0 = 4.4$, $\bar{x}_1 = 2.9$ and $\phi = 0.15, \gamma = 0.05$, and $\omega = 3.5$. Varying the remaining parameter f_0 we obtain a bifurcation diagram for Eq.(2.17) (see Fig.2.7). As f_0 is decreased there is a type iii intermittency transition to chaos [similar to the map (2.15)]. For $f_0 = 4.0$ the average lifetime of a chaotic transient is $\tau = 12.0$. In order to estimate $\langle h_\perp \rangle$ we integrated the equations for the tangent vector representing
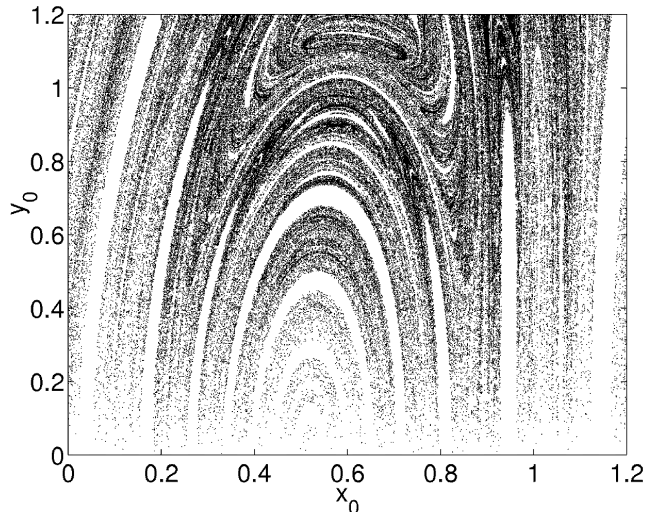
Figure 2.8: Numerical basin for (2.16) obtained on 1000×1000 initial conditions. We iterate each initial condition forward in time until the trajectory either gets very close to the invariant plane $y = 0$ ($|y| < 10^{-8}$, $|v_y| < 10^{-9}$, and $y \cdot v_y < 0$), or else is definitely in the repelling region ($|y| > 20$, $|v_y| > 100$, and $y \cdot v_y > 0$). Black dots correspond to initial conditions eventually attracted to ∞.

$\langle h_\perp \rangle$	D	α_{th}	α_{exp}
0.030	0.0285	1.26	1.29

Table 2.3: Data for Example 3.

the infinitesimal variations from the invariant plane $y = v_y = 0 : d\delta y/dt = -\gamma \delta v_y - 2(x + \bar{x})\delta y, d\delta y/dt = \delta v_y$, where δy and δv_y are infinitesimal variations (2.8). The results are presented in Table 2.3 and we again find reasonably good agreement between our estimates of α_{th} and α_{exp}.

2.5   Conclusion

In this paper we have considered systems with an invariant manifold in which are located both a nonattracting chaotic set and a nonchaotic attractor (e.g., a

periodic orbit). Thus, in this situation, typical initial conditions in the invariant manifold may yield orbits that experience chaotic transients before approaching the chaotic attractor. It is found that the basin boundary separating the basins of the attractor in the invariant manifold and another attractor not in the invariant manifold is characterized by stalactite like structure, thin cusp-shaped regions extending down to touch the invariant manifold at the location of points in the nonattracting chaotic set. Using a random walk model, we have obtained a scaling relation for the variation of the measure of the basin of the attractor not in the invariant manifold. In particular, we show that this basin's measure in a surface at a small distance y from the invariant manifold scales as a power law y^α, and we have obtained a theoretical prediction for the scaling exponent α. This prediction has been tested with good results by comparison with various numerical experiments.

Appendix

The solution to Eq.(2.7) subject to the boundary condition $\bar{P}(0, \bar{y}_1, s) = 0$ is

$$
\bar{P}(\bar{y}, \bar{y}_1, s) = \begin{cases} A(\exp[-\kappa_a \bar{y}] - \exp[\kappa_b \bar{y}]), & 0 < \bar{y} < \bar{y}_1, \\ B \exp[-\kappa_a \bar{y}], & \bar{y} > \bar{y}_1, \end{cases} \tag{2.18}
$$

where

$$\kappa_a = \frac{1}{2D}\left(\sqrt{\langle h_\perp \rangle^2 + 4D(s + 1/\tau)} + \langle h_\perp \rangle\right),$$

$$\kappa_b = \frac{1}{2D}\left(\sqrt{\langle h_\perp \rangle^2 + 4D(s + 1/\tau)} - \langle h_\perp \rangle\right),$$

$$A = -\frac{\exp[-\kappa_b \bar{y}_1]}{(\kappa_a + \kappa_b)D},$$

$$B = -\frac{\exp[-\kappa_b \bar{y}_1] - \exp[\kappa_a \bar{y}_1]}{(\kappa_a + \kappa_b)D}.$$

Thus

$$
\begin{aligned}
\int_0^\infty \bar{P}(\bar{y}, \bar{y}_1, s)d\bar{y} &= \int_0^{\bar{y}_1} \bar{P}d\bar{y} + \int_{\bar{y}_1}^\infty \bar{P}d\bar{y} \\
&= A[(1 - \exp[-\kappa_a \bar{y}_1])/\kappa_a - (\exp[\kappa_b \bar{y}_1] - 1)/\kappa_b] + B\exp[-\kappa_a \bar{y}_1])/\kappa_a \\
&= \frac{1 - \exp[-\kappa_b \bar{y}_1]}{s + 1/\tau}.
\end{aligned}
$$

Finally,

$$
\begin{aligned}
P_{y=0} &= \frac{1}{\tau}\int_0^\infty \int_0^\infty P(\bar{y}, \bar{y}_1, n)d\bar{y}dn \\
&= \frac{1}{\tau}\int_0^\infty \bar{P}(\bar{y}, \bar{y}_1, 0)d\bar{y} \\
&= 1 - \exp[-\alpha \bar{y}_1] = 1 - y_1^\alpha,
\end{aligned}
$$

where α is κ_b with s set equal to zero. Thus

$$P_\infty = 1 - P_{y=0} = y_1^\alpha,$$

which is Eq.(2.10).

Chapter 3

Time-delayed feedback dynamical systems and their application to communications

3.1 Communication with a Chaotic Traveling Wave Tube Microwave Generator

3.1.1 Introduction

[1] In the system we envision, the signal sent by the transmitter is generated by a traveling wave tube (TWT) oscillator [6–8] operating in the chaotic regime. That is, under the supposed operating conditions, the TWT naturally produces a narrow band microwave signal with temporally chaotic phase and amplitude variations. We show that, if suitable small perturbations are applied to the TWT, the symbolic dynamics of the chaotic TWT can be controlled. Following the idea of Hayes et al. [25,26], the information being transmitted is encoded in

---

[1]Section 3.1 is a verbatim representation of the paper by Vasily Dronov, Matthew R. Hendrey, Thomas M. Antonsen, Jr., and Edward Ott, Communication with a Chaotic Traveling Wave Tube Microwave Generator, published in *Chaos* 14, 30 (2004).

the controlled symbolic dynamics of the chaos.

Detection of the signal at the receiver can be accomplished by use of a replica of the transmitter's chaotic TWT oscillator. The small received signal is amplified by the replica receiver system through the phenomenon of synchronization of chaos [2]. This provides a potentially simple, cheap, and compact amplifier for the detector system, which is only possible because the original signal was produced by a chaotic system. A notable feature of this scheme is that, in the ideal case, the signal amplification is in principal distortionless, even though the process is nonlinear (the nature of distortionless amplification is explained in Sec. 3.1.5). In applications where the benefits of receiver simplicity and compactness are paramount (e.g., satellite-based communication), our scheme may provide advantage.

In Sec. 3.1.2 we describe a model for a TWT feedback oscillator. In Sec. 3.1.3 we investigate this model through numerical simulations, display its chaotic behavior and characterize this behavior. Section 3.1.4 discusses how, following the scheme of Refs. [25, 26], information can be encoded in the TWT oscillator output through control of the symbolic dynamics of the chaos. Section 3.1.5 discusses the possibility of using the phenomenon of synchronization of chaotic systems for the purpose of efficiently amplifying and retransmitting a chaotic signal of the type discussed in Sec. 3.1.4. A noise analysis of such a chaos-based communication system is given in Sec. 3.1.6. Section 3.1.7 presents further discussion and summarizes our conclusions.

Finally, we wish to emphasize that our motivation for considering TWT oscillator operation in the chaotic regime is the possibility of attaining improved power efficiency and device compactness. In particular, unlike some other work
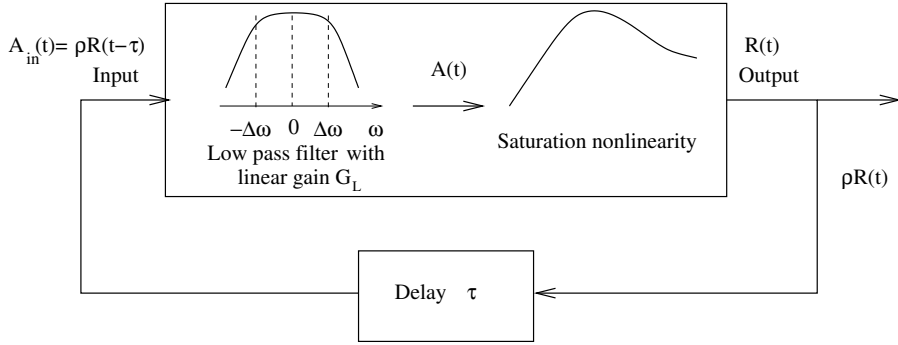
Figure 3.1: Schematic of the free-running chaotic oscillator.

using chaos in communications [31, 32], secrecy is not one of our goals.

3.1.2 The Model

In this section we review a model for the nonlinear operation of a TWT which can be made to oscillate by adding feedback. We model the TWT in the following way. Assume that the signal at the input is $A_{in}e^{i\omega_c t}$ where $A_{in}(t)$ is the complex envelope of the signal and ω_c is the carrier or reference frequency. The linear behavior of the tube is modeled as a first-order bandpass filter with the bandwidth $2\Delta\omega$, centered near the carrier frequency. The linear gain of the filter is G_L. Nonlinearity arises due to power saturation as the electron beam bunches toward the output end of the TWT. A small fraction ρ of the output is then fed back into the the input through a feedback line with delay time τ. Performing a frequency shift $\omega \to \omega - \omega_c$ we translate the analysis to low frequency (i.e. $A_{in}e^{i\omega_c t} \to A_{in}$) so that the time variation of the complex variable A_{in} represents the slow amplitude and phase modulation of $\text{Re}[A_{in}e^{i\omega_c t}]$. A schematic diagram of the model in this low-frequency representation is shown in Fig.3.1.

34

The input $\bar{A}_{in}(\omega)$ and the output $\bar{A}(\omega)$ of the first-order low-pass filter with the bandwidth $2\Delta\omega$ are related by

$$\bar{A}(\omega) = \frac{G_L \bar{A}_{in}(\omega)}{1 + i\omega/\Delta\omega}$$

and, therefore,

$$\bar{A}_{in}(\omega) = \frac{\bar{A}(\omega)(1 + i\omega/\Delta\omega)}{G_L},$$

in the frequency domain, and

$$A_{in}(t) = \left[(\Delta\omega)^{-1}\frac{d}{dt} + 1\right]\frac{A(t)}{G_L},$$

in the time domain. In general the frequency dependence of the linear transfer function for a TWT is more complicated than a simple first order band pass filter. We adopt the first order band pass filter here because that is the simplest model giving a nonzero memory time. Since TWT amplifiers are broadband, our model can be realized by inserting a narrow band first order filter in the signal path. The TWT output (Fig.3.1) is

$$R(t) = A(t)\frac{e^{i\eta|A(t)|^2}}{1 + |A(t)|^2}, \tag{3.1}$$

where the term $[\exp{(i\eta|A(t)|^2)}][1 + |A(t)|^2]^{-1}$ models the nonlinearity of the TWT with η being a parameter characterizing the quadratic phase nonlinearity, and the coefficient of $|A(t)|^2$ in the denominator of (3.1) can be set to one using a suitable normalization of $A(t)$. This model of the nonlinearity is one of a class of models due to Saleh [18] which have been used in the community [19] to simulate communications systems with TWT's. Since $A_{in}(t) = \rho R(t - \tau)$, the equation for $A(t)$ becomes

$$\frac{dA(t)}{dt} + A(t) = kA(t - \tau)\frac{e^{i\eta|A(t-\tau)|^2}}{1 + |A(t-\tau)|^2}, \tag{3.2}$$

where k is the loop gain, $k = \rho G_L$, and the bandwidth $\Delta\omega$ has been normalized to unity by means of a rescaling of the time variables, i.e., $t \to t\Delta\omega$ and $\tau \to \tau\Delta\omega$.

Note that our modeling of a TWT as consisting of linear and nonlinear stages (as illustrated in Fig.3.1) is only an approximation and that such a sharp decomposition does not truly exist. Nevertheless, it has been found [18, 19] that Eq.(3.2) is very effective at modeling real TWT experiments. Also note that the model variable $A(t)$, the output of the fictious linear stage, is not a measurable physical quantity, but that $R(t)$, given in Eq.(3.1) in terms of $A(t)$, does represent a measurable physical quantity.

It is also important to mention that, while a wide variety of TWT models exist [8, 18, 19] with varying complexity [20–22], the unique property of our model is that it is perhaps the simplest that is able to describe the behavior of a TWT oscillator with feedback.

3.1.3 Chaotic Behavior

The right-hand side of Eq.(3.2) contains a delayed argument $A(t-\tau)$. Thus (3.2) is an infinite dimensional dynamical system (to evolve $A(t)$ forward from $t = \tau$, we must specify the *function* $A(t)$ in $0 \leq t \leq \tau$). The dynamics of the system can, however, be finite dimensional or even low dimensional. In particular, the system state may asymptote to a low dimensional subset of the infinite dimensional state space. This subset is called an attractor. We are interested in the case where the system motion on the attractor is chaotic. In the case of low dimensional chaotic dynamics, it is often feasible to find a phase space partition and the corresponding symbolic dynamics for the chaotic attractor. However, there is no

common recipe for finding a parameter set that makes the dynamics chaotic and low-dimensional. A powerful tool that can be helpful in this situation is the set of Lyapunov exponents for the system. Our goal is to arrive at a situation where the largest Lyapunov exponent is positive (yielding chaos) while others are either zero or negative (in order to provide contraction of the flow in the directions normal to the expansion direction).

In order to compute the Lyapunov exponents we consider an infinitesimal variation from $A(t)$, denoted $\delta A(t)$. Equation (3.2) yields the following linearized equation for δA,

$$
\begin{aligned}
\frac{d[\delta A(t)]}{dt} + \delta A(t) \; = \; & k \frac{e^{i\eta|A(t-\tau)|^2}}{1 + |A(t-\tau)|^2} \\
\times \; & \left[\delta A(t-\tau) + A(t-\tau)\{i\eta - \frac{1}{1 + |A(t-\tau)|^2}\} \right. \quad (3.3) \\
\times \; & \left. \{A(t-\tau)\delta A^*(t-\tau) + A^*(t-\tau)\delta A(t-\tau)\} \right],
\end{aligned}
$$

where δA^* is the complex conjugate of δA. In order to compute the first N exponents, we start with N unit norm orthogonal functions $\delta A_i = u_i$ on the interval $[0, \tau]$, i.e.,

$$
\left(u_i(t), u_i(t) \right) = \|u_i(t)\|^2 = \frac{1}{\tau} \int_0^\tau \{\mathrm{Re}[u_i(t)]\mathrm{Re}[u_i(t)] + \mathrm{Im}[u_i(t)]\mathrm{Im}[u_i(t)]\}dt = 1,
$$

$$
\left(u_i(t), u_j(t) \right) = \frac{1}{\tau} \int_0^\tau \{\mathrm{Re}[u_i(t)]\mathrm{Re}[u_j(t)] + \mathrm{Im}[u_i(t)]\mathrm{Im}[u_j(t)]\}dt = 0, \text{ for } i \neq j.
$$

Following the procedure described, for example, in Ref. [23], p. 148, we integrate (3.3) with these initial conditions and periodically use a Gram-Schmidt algorithm to renormalize the functions δA_i, keeping them orthogonal as we integrate the flow forward in time. The i'th Lyapunov exponent λ_i is computed as the average rate of exponential growth of the norm of the function $\delta A_i(t)$, i.e.,
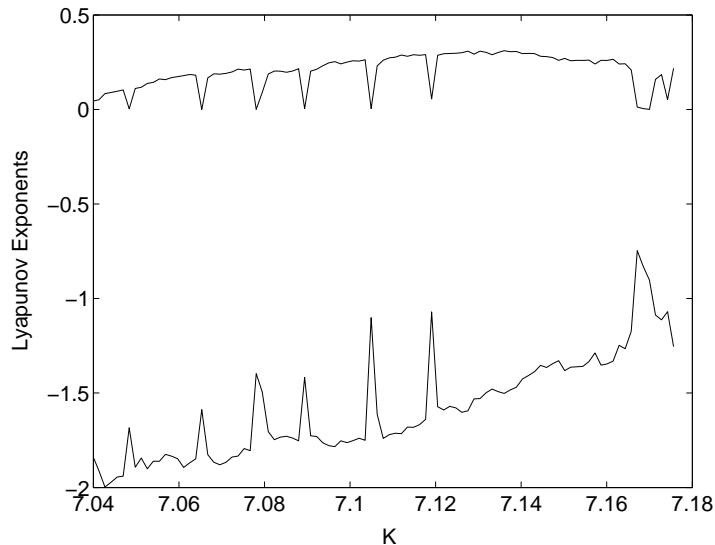
Figure 3.2: Lyapunov exponents as functions of k, $\tau = 0.530$ and $\eta = 1.0$.

$\lambda_i = \lim_{T \to \infty} \frac{1}{T} \log \left[\|\delta A_i(T)\| / \|\delta A_i(0)\| \right]$, where the subscript label i is chosen so that $\lambda_1 \geq \lambda_2 \geq \lambda_3 \geq \ldots$.

Figure 3.2 shows results of a computation of the first four Lyapunov exponents for τ and η fixed and k varied. Only the positive and least negative exponents are plotted. Two other exponents are identically zero by virtue of the invariance of Eq.(3.2) under time translation and under change of the phase of A [i.e., $A \to A\exp(i\varphi)$, where φ is a constant]. In Fig.3.3(a) we show $|R(t)|$ versus $|R(t-7\tau/4)|$ for $k = 7.142, \tau = 0.530, \eta = 1.0$. Figure 3.3(b) shows the return map $|R_{m+1}| = f(|R_m|)$, where $|R_m|$ is the value of $|R(t)|$ at the m-th passage of $|R(t_m - 7\tau/4)|$ through the value 0.425 going from left to right (i.e., $d|R(t - 7\tau/4)|/dt > 0$ at $t = t_m$). We note that the return map is nearly one-dimensional, indicating that the dimension of the attractor in Fig.3.3(a) is near (but slightly bigger than) two.

3.1.4   Encoding Information via Controlling Chaos

A. Choosing a partition and an appropriate set of symbols

38
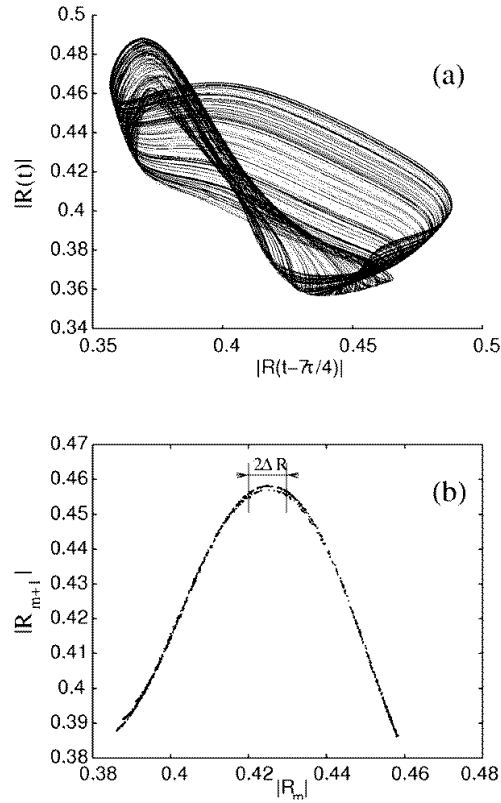
Figure 3.3: (a): Uncontrolled attractor for $k = 7.142$, $\tau = 0.530$ and $\eta = 1.0$. (b): Return map for the same attractor using the surface of section $|R(t - 7\tau/4)| = 0.425$.

Partitions give a rule which assigns a symbol whenever the state is in a certain portion of the phase space. For the return map in Fig.3.3(b), a natural way to choose the partition is to divide the map at its maximum, so that the left side corresponds to "0" and the right-hand side to "1". Such a partition rule is often called a *two-level quantizer*. Note however, that this partition rule is not robust with respect to assigning correct symbols near the maximum of the curve; i.e., noise or a small error in measuring $|R_m|$ will result in an incorrect symbol assignment. To make our communication system robust to noise, we will

39

introduce a "noise-resisting gap" (Sec.3.1.4C). That is, we restrict the dynamics so that the orbit never falls within an interval of width $2\Delta R$ centered at the maximum of the curve in Fig.3.3(b). (e.g., [24].)

B. Learning the grammar of the symbolic dynamics of the system (which symbol sequences are allowed)

Starting off with a particular value of $|R_m|$ and iterating the map $N-1$ times forward, one obtains a binary string of length N; examining many such strings originating from different initial conditions gives the collection of binary strings of length N allowed by the dynamics. Such a collection forms the symbolic grammar of the system. In what follows, to transmit a message consisting of an arbitrary sequence of bits, we code the message in such a way that in can be represented as a different bit string (possibly of length greater than its original length) such that any substring of length N (with N suitably chosen) within this new string does not violate the grammar restrictions of the free running system.

C. Encoding information by means of controlling the symbolic dynamics

For dynamics as in Fig.3.3, techniques for encoding binary data by controlling chaos have been described in a number of papers [24–27]. The main idea is to utilize the exponential divergence of the flow by applying tiny perturbations to the system in such a way as to cause a prescribed symbolic sequence to be followed.

The method can be split into two parts [24–26]:

- *Learn the dynamics of the free-running system*

  Letting the flow for our system (3.2) evolve in time, we record $|R_m|$ along with the bit string of length N following this $|R_m|$. (In our numerical examples we use $N = 5$.) A convenient way to represent this bit string is to

assign to $|R_m|$ an integer number n between 0 and $2^N - 1$. For our system all the $|R_m|$'s leading to the same bit sequence n fall within a narrow interval. Taking the averages $s(n)$ of the $|R_m|$ values in the interval corresponding to n, we obtain a table $s(n)$. Thus, if we can set $|R|$ to $s(n)$, the orbit will follow the bit sequence n on the surface of section. For example, in the case when we are willing to increase immunity to noise by means of using a "noise-resisting gap", we only consider bit strings of a length N that never enter the gap. This, of course, introduces additional grammar restrictions. For example, in the case where the gap width is $2\Delta R = 0.01$, the sequence "00000" must be ruled out when message coding is done.

- *Learn the dynamics of the perturbed system*

  We now apply a small reference perturbation of amplitude p_{ref} to the system after every N crossings of the surface of section. Following an orbit for a long time, we record the values of $|R_m|$ just before the perturbation and note the bit string n that they lead to. Averaging such values we obtain a second table, $w(n)$. Thus the quantity $w(n)$ is simply a perturbed version of $s(n)$. In our numerical experiments the reference perturbation is a small pulse of fixed duration and amplitude applied to the input of the TWT. Having found $s(n)$ and $w(n)$ and assuming that the effect of the small perturbation is linear, we now make the orbit follow a desired sequence n_0 by applying a perturbation of amplitude

  $$p = [|R_i| - s(n_0)]d(n_0),$$

  where

  $$d(n) = \frac{p_{ref}}{w(n) - s(n)}.$$

Binary
Input
$\rightarrow$ .r r r r r r r ...
         1 2 3 4 5 6 $\rightarrow$

Bernulli Shift at $t=t_n$

Controller
$p_r = d(r)[s(r) - |R(t_n)|]$

where $r = \sum_{i=1}^{5} r_i \, 2^{5-i}$

$R(t_n)$

Poincare surface
of section at times t_n
$|R(t_n - 7\tau/4)| = 0.425$

$1 + p_r$

X

$\rho R(t-\tau)$

$-\Delta\omega$ 0 $\Delta\omega$ ω
Low pass filter with
linear gain G_L

$A(t)$

Saturation nonlinearity

$R(t)$

Output
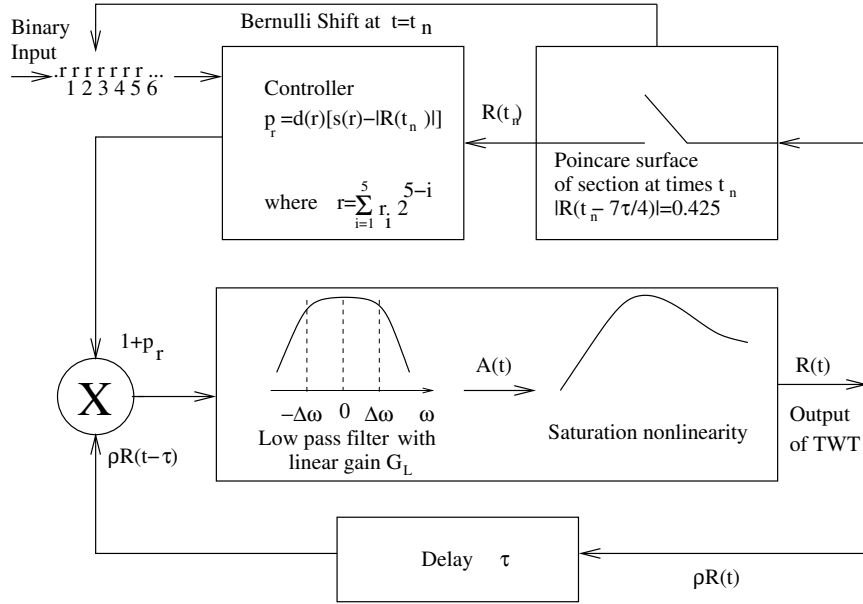of TWT

Delay τ

$\rho R(t)$

Figure 3.4: Schematic of the controller.

An overall view of the encoding scheme is represented pictorically in Fig.3.4. The controlled attractor is shown in Fig.3.5. Note that by construction, any segment of the controlled orbit of a length N (and, therefore, the whole orbit) avoids the noise-resisting gap of width $2\Delta R$ indicated in Fig.3.3(b). Therefore, the controlled orbit will also avoid all the post images of that gap. Thus, as compared to the attractor in Fig.3.3, the controlled attractor (Fig.3.5) is permeated by gaps.

3.1.5 Synchronization and Retransmission

TWT's are commonly used in satellite communication systems. As an example, we imagine that the encoded chaotic signal generator described in Sec. 3.1.4 is transmitting from a ground-based station to a satellite. We wish to receive a signal on the satellite, amplify it, and retransmit it back to the ground. In our communication system we attempt to use another TWT that is an identical
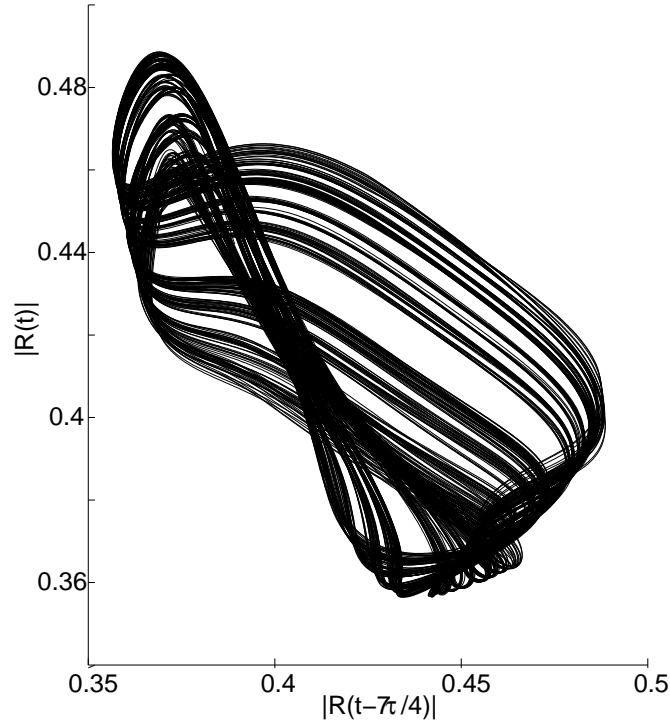
Figure 3.5: Controlled attractor for $N = 5$ and gap-size $2\Delta R = 0.01$. A random sequence of bits was used for generating the message.

(or nearly identical) replica of the original TWT to amplify and retransmit the received signal. Using a low power pre-amplifier, we envision restoring the signal from the receiving antenna to the (small) amplitude ρR at the input of the transmitting TWT. Ideally (in the absence of noise and channel distortion) the input to the TWT on the ground (from the feedback) and the TWT on the satellite (from the preamplifier) will be identical. Thus they produce identical outputs, and the TWT on the satellite accomplishes distortionless amplification to high power even though it is operating in a fully nonlinear regime. (This scheme may be regarded as a variant on ideas related to synchronization of chaotic systems [2, 31, 32].)

$\hat{Q}(m)$

Two–level quantizer

$\hat{R}(t_m)$

Poincare surface
of section at times t_m
$|R(t_m-7\tau/4)|=0.425$

Binary
output

Input
$\rho R(t-\tau)$

Σ

$+$

$+$

Noise

$-\Delta\omega$ $\;0\;$ $\Delta\omega$ $\quad\omega$
Low pass filter with
linear gain G_L

$\hat{A}(t)$
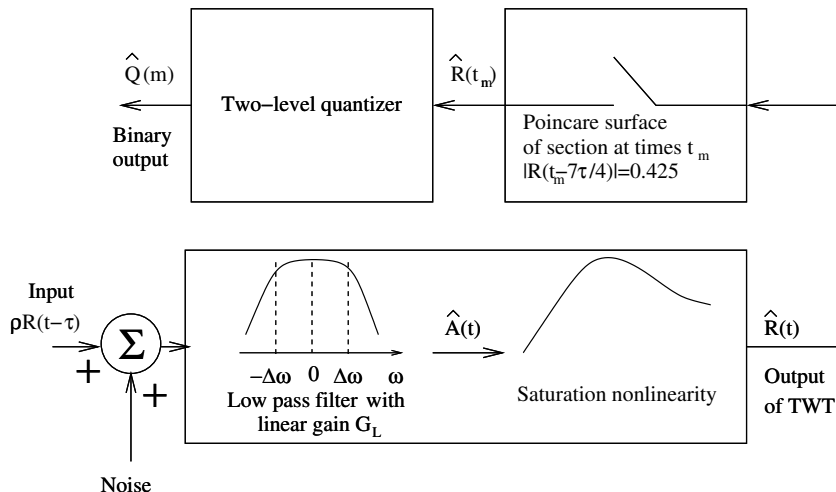
Saturation nonlinearity

$\hat{R}(t)$

Output
of TWT

Figure 3.6: Schematic of the receiver.

Note that this type of synchronism-based system is only possible because our information-bearing controlled signal is one of the naturally occurring chaotic orbits of the original transmitting TWT. We have also tested the robustness of our amplification scheme to noise (see Chapter 3.1.6).

We believe that such a system offers potential advantages with respect to compactness, an important consideration for a satellite system where weight is a prime concern. Also, there is some indication that TWT's operated in the chaotic regime may have enhanced power efficiency as compared to TWT's operating in their stable linear range [7]. This again may be advantageous since the need for expulsion of waste heat from the satellite is lessened.

3.1.6   Noise Analysis

We consider three issues: (1) bandwidth efficiency, (2) bit error rate (BER) dependence on signal-to-noise ratio (SNR), and (3) the effect of synchronization on SNR.
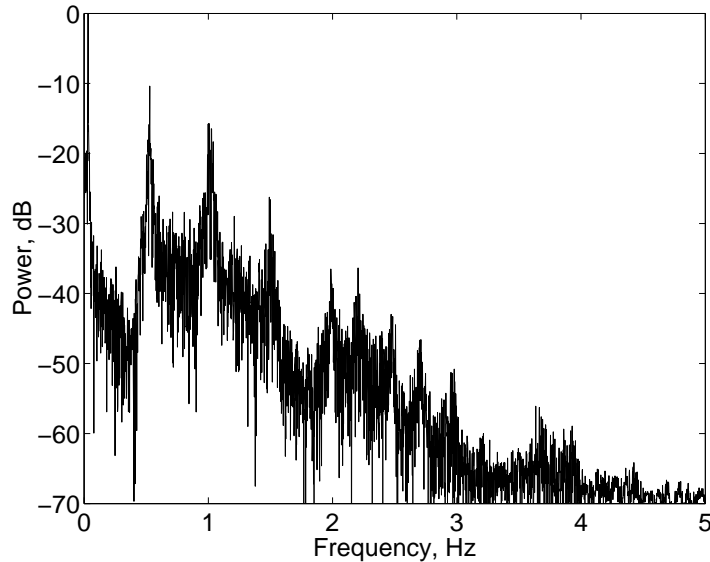
Figure 3.7: Normalized power spectral density of the transmitted signal.

(1) *Bandwidth efficiency.*

Bandwidth efficiency is defined as the ratio of the bit rate to the signal bandwidth. The bit rate is determined by the number of crossings of the Poincare plane per unit time and is approximately 0.5 bits per unit of our normalized time variable; the bandwidth can be estimated as the portion of power spectrum of the signal (see Fig.3.7) containing 99% of total power, which is approximately 1. Therefore, the bandwidth efficiency is approximately 0.5. For comparison, the bandwidth efficiency of a binary PSK (phase shift keying) [45] or FSK (frequency shift keying) [45] modulated signal is 0.5. Thus, our scheme uses bandwidth at least as efficiently as some traditionally used modulation techniques. (Detailed information on different types of modulation techniques and their properties can be found in [45].)

(2)*BER dependence on SNR.*

An upper bound for BER (assuming that "0"'s and "1"'s are equally likely to

occur) is derived in the appendix and is given by

$$P_e \leq \frac{1}{2}\text{erfc}\left(\frac{\Delta\hat{R}}{\sqrt{N_0 f_B}}\right) < \frac{e^{-\frac{(\Delta\hat{R})^2}{N_0 f_B}}}{2\sqrt{\pi}},$$

where f_B is the bandwidth of the signal, $\Delta\hat{R}$ is a noise-resisting gap of the received chaotic attractor (signal), and N_0 is the noise power spectral density at the receiver input. Thus the BER becomes very small for $(\Delta\hat{R})^2 \gg N_0 f_B$. Note that $N_0 f_B$ represents the effective power of the interfering signal (noise), whereas $(\Delta\hat{R})^2$ is determined by the relative size of the noise-resisting gap as well as the overall size of the chaotic attractor (signal strength or power, speaking in practical terms) at the receiver input. Therefore, there exist two ways of improving BER performance: boosting the signal power, and increasing the relative size of the noise-resisting gap. A bigger gap requires a more restricted symbolic dynamics; therefore, less data can be sent. While the output power of TWT is limited by its physical design, the gap size can be controlled by altering the symbolic dynamics [24] of the TWT, and therefore, offers a rather flexible means of tuning a chaotic TWT for either better BER performance or higher data rate.

(3)*Effect of synchronization on SNR.*

In our numerical tests we added to the chaotic signal a filtered low-frequency Gaussian noise component with a frequency bandwidth of approximately 1. In this case, the cutoff frequency of the linear component in our TWT model (see Fig.3.1) will lie beyond the bandwidth of the noise component, and therefore, the linear low-pass portion of our TWT model will not filter incoming noise. In this scenario, any improvement in BER performance must be attributed to the effect of synchronization. Numerical simulations show that the SNR after synchronization (SNR at the output of the receiving TWT vs. SNR at the receiving antenna) increases by approximately 11.3 dB.
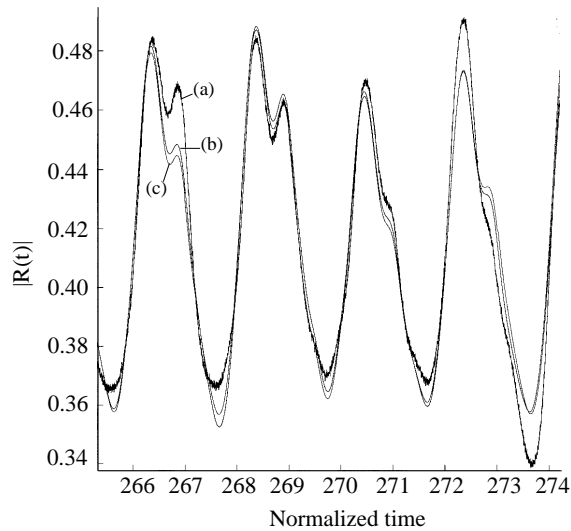
Figure 3.8: Time series of: (a) noisy chaotic signal, (b) chaotic signal prior adding noise, and (c) signal filtered by means of chaotic synchronization (c). One can clearly see that time series (c) and (b) look almost indistinguishable, eventhough time series (a) is quite different.

Another set of numerical simulations showed that the BER at the output of the synchronized TWT was an order of magnitude less than that at the input of the receiving TWT for an input SNR equal to 32 dB. The time series that illustrates the effect of synchronization are shown in Fig.3.8.

An important issue relevant to the overall performance of our communication scheme concerns the optimal gap size ΔR. As we have shown earlier, ΔR can be viewed as a variable that allows one to optimize a given chaotic communication system for a particular application, or meet certain design constraints. One such constraint could be a given threshold for BER. Another constraint could be to maximize information throughput (data with no errors) of the TWT-based chaotic communication system. Unfortunately, there is no clear relation between information throughput and the size of ΔR. Although increasing ΔR greatly improves robustness to noise, the entropy of the map describing dynamics of the

TWT decreases, and the effective data rate in the communication system also decreases. On the other hand, the Channel Coding Theorem [45] states that there exists an error control coding algorithm such that the probability of an error can be made smaller than any $\epsilon > 0$ provided that the code rate is smaller then channel capacity C. In other words, the channel capacity C determines an upper bound on the amount of error-free information that can be sent through the channel. So the answer can be found by looking at the gap size, bit rate, and SNR in a more general way: the optimum gap size in this case would simply maximize the channel capacity C for a given value of the noise power density at the receiver input.

To summarize the results of this section, we addressed two key components of communication system design, bandwidth efficiency and performance in a noisy environment. We also identified a mechanism that can be used to optimize the performance of the proposed communication system.

3.1.7 Future Work

Summarizing our work, we have developed a model of a proposed chaotic communication system where controlling chaos is used as an alternative means of "modulation" for encoding of binary information. We have shown using numerical simulations that, while the proposed communication system in some aspects behaves as good as conventional ones, it also offers potentially new benefits.

We believe that our work may be relevant in situations where the main concern is increase of the compactness and power efficiency of the amplifier (as, for example, in the case where the amplifier is on a space satellite).

While traditional modulation techniques, such as PSK (phase shift keying)

and QAM (quadrature amplitude modulation) [45], allow avoidanceof unmodulated spectral components and, therefore, achieve high power efficiency, these techniques can only be used with linear TWTs. On the other hand, TWT's in general are known to be more power efficient when operating in the nonlinear regime, when chaotic modulation can be utilized.

A qualitative analysis of the chaotic attractor in Fig. 3.5 reveals that the chaotic flow produced by our model can be characterized by small relative amplitude variation and absence of rapid transitions in phase. As a result, a large fraction of spectral power is being contained in the periodic (unmodulated) spectral component. In contrast, conventional modulation techniques, such as QAM and PSK, are characterized by fast transitions in phase, which allows utilization of the transmitted energy in a very efficient manner.

We note, however, that the large unmodulated component in our numerical example is a characteristic of our particular example and not of the general proposed method. Thus it remains a problem for future study to find and characterize chaotic TWT operation that yields chaotic signals that have a smaller unmodulated component [46].

Thus, it is not yet clear whether *overall* performance of the chaotic satellite communication system that we propose is better than that of traditionally used ones. A clear answer to this question awaits experimental implementation and test of our proposed system [46].

3.1.8 Appendix: derivation of the upper bound for BER

Let $\hat{R}$ be a "modulated" chaotic signal $R(t)$ received by the second TWT. Clearly, $\hat{R}$ will be considerably attenuated. Therefore, the new attractor obtained from $\hat{R}$
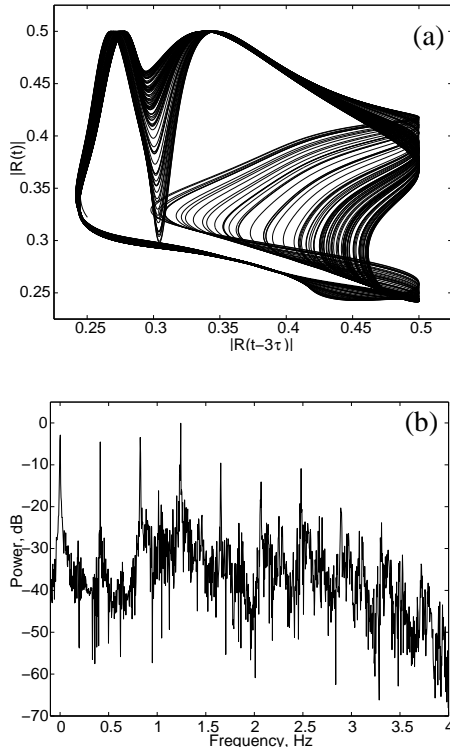
Figure 3.9: (a): Attractor obtained from the second order model for $k = 14.855$, $\tau = 0.5313$ and $\eta = 0.725$. (b): Normalized power spectral density for the second order model for the same set of parameters

will be a scaled-down version of the one in Fig.3.5. Sampling the values of $|\hat{R}(t_n)|$ at the surface of section of the new attracor obtained from the received signal and comparing them to the value of $\hat{R}$ at the middle of its noise resisting gap, one interprets $|\hat{R}(t_n)|$ either a "0" or a "1". Due to noise in the channel, some of the bits in the receiver will be read incorrectly. We are going now to estimate the fraction of incorrectly transmitted bits or BER.

For convenience, in the following, we regard the receiving TWT as acting like a linear amplifier (i.e., we neglect the nonlinearity in (3.2)). Suppose that white Gaussian noise $w(t)$ with the power spectral density $N_0/2$ is added to the signal at the receiver input. We model the effect of the slow wave structure

of the receiving TWT as a first-order low-pass filter. What we sample at the output of the receiving TWT is a true signal $|\hat{R}(t_n)|$ plus $y(t_n)$, where $y(t) = \int_{-\infty}^{\infty} h(\tau)w(t - \tau)d\tau$. For the first-order low-pass filter with cutoff frequency ω_0, $h(t) = \omega_0 u(t)e^{-i\omega_0 t}$, where $u(t)$ is a step function. Now we make another assumption; we assume that, in the absence of noise, $|\hat{R}(t_n)| = \hat{R}_{\pm} = \lambda \pm \Delta\hat{R}$. In other words, we assume that the signal is always measured at the edge of the noise-resisting gap, where the value of the measured signal is closest to the threshold λ and, thus errors are the most likely to occur. Therefore, we are going to estimate an upper bound for the BER. Since errors occur due to $y(t)$, and since $y(t)$ is a Gaussian process, we would like to find the variance of $y(t)$.

$$
\begin{aligned}
\sigma_y^2 = E[y^2] &= \omega_0^2 E\left[\int_0^{\infty}\int_0^{\infty} e^{-\omega_0\tau_1}e^{-\omega_0\tau_2}w(t - \tau_1)w(t - \tau_2)d\tau_1 d\tau_2\right] \\
&= \omega_0^2 \int_0^{\infty}\int_0^{\infty} e^{-\omega_0\tau_1}e^{-\omega_0\tau_2} E[w(t - \tau_1)w(t - \tau_2)]d\tau_1 d\tau_2 \\
&= \omega_0^2 \int_0^{\infty}\int_0^{\infty} e^{-\omega_0\tau_1}e^{-\omega_0\tau_2} R_w(t - \tau_1, t - \tau_2)d\tau_1 d\tau_2.
\end{aligned}
$$

The autocorrelation function of $w(t)$ is $R_w(\tau_1, \tau_2) = N_0/2\delta(\tau_1 - \tau_2)$, so the integral above becomes:

$$
\sigma_y^2 = \omega_0^2 \int_0^{\infty} e^{-2\omega_0\tau_1}d\tau_1 = \frac{N_0\omega_0}{4}.
$$

Remembering that $y(t)$ is a Gaussian process, the pdf of $\hat{R}_{\pm} + y(t_n)$ can be expressed as

$$
f_{\hat{R}_{\pm}}(y) = \frac{1}{\sqrt{\pi N_0\omega_0/2}} \exp\left(\frac{-(y + \lambda \pm \Delta\hat{R})^2}{N_0\omega_0/2}\right) \text{ (see Fig.3.10)}.
$$

Here $\pm$ refers to the condition that a "1" or a "0" was transmitted ($\hat{R}_+ + y(t_n)$ or $\hat{R}_- + y(t_n)$ was received, respectively).
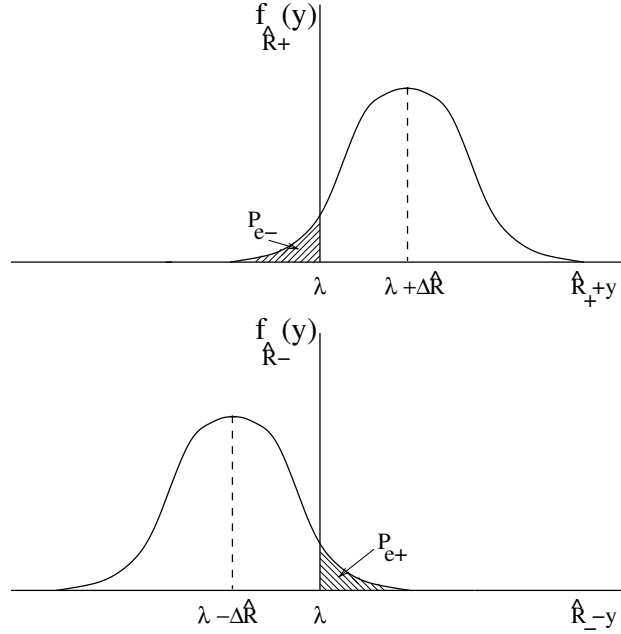
Figure 3.10: Distribution of the signal sampled at the output of the low-pass filter with the cutoff frequency ω_0.

For the case of non-coherent detection (when we do not know at what times the signal needs to be sampled), the effective width of a Gaussian becomes twice of that of the coherent case described above. Therefore,

$$f_{\hat{R}_\pm}^{noncoh}(y) = \frac{1}{\sqrt{\pi N_0 \omega_0}} \exp\left(\frac{-(y + \lambda \pm \Delta\hat{R})^2}{N_0 \omega_0}\right).$$

The probability of an event in which the received symbol is different from what was transmitted is

$$P_{e\pm} = \int_\lambda^{\pm\infty} f_{\hat{R}_\pm}(y) dy = \frac{1}{\sqrt{\pi N_0 \omega_0}} \int_\lambda^{\pm\infty} \exp\left(\frac{-(y + \lambda \pm \Delta\hat{R})^2}{N_0 \omega_0}\right) dy.$$

Performing integration one gets a rather simple answer:

$$P_e = P_{e\pm} = \frac{1}{2}\text{erfc}\left(\sqrt{\frac{(\Delta\hat{R})^2}{N_0 \omega_0}}\right). \tag{3.4}$$

The equation (3.4) gives an upper bound for BER.

3.2 Using Time-Delayed Electronic Circuits for Secure Communications

3.2.1 Introduction

Introduction

There are many examples where chaotic dynamical systems can operate as a communication system [11, 15, 17, 28, 29, 31–34]. Chaotic signals possess certain properties that can make use of chaos advantageous. One such property of chaotic signals is wide-spreading in the frequency domain which makes their performance superior in a multipath environment. Another property which might be beneficial is the complex structure of chaotic signal. It has been shown [28] that high-dimensional chaotic waveform behaves very much like a random signal, i.e., its autocorrelation function is very sharp. This suggests the idea of using chaos for secure communication. Mixing such a waveform with a small information-bearing signal would mask the latter, providing, therefore, security to a certain extent. On the receiving end, where parameters of the dynamical system generating chaos are known, information-bearing signal can be separated from chaotic carrier by making use of the chaos synchronization phenomenon. The phenomenon of chaotic synchronization was described for the first time by Afraimovich et al [1] and later applied to secure communications by Carrol and Pecora [2]. Their approach, however, is not free of drawbacks. The main problem with their scheme is an occasional desynchronization which leads to errors, even when communication channel is ideal.

A different approach was proposed by Volkovskii and Rulkov, which is characterized by so-called open loop coupling. To clarify this approach, let us assume

the the dynamics of the chaotic transmitter is described by the following equation:

$$\dot{x}(t) + x(t) = F(x(t - \tau)).$$

In this scheme, the information-bearing message $s(t)$ is injected into the state of transmitting system as follows:

$$\dot{x}(t) + x(t) = F(x(t - \tau) + s(t)).$$

The quantity $z(t) = x(t-\tau) + s(t)$ is then sent through the channel. The message is then recovered by estimating the state variable $x(t)$, and subsequently, the encoded message $s(t)$ in the receiver:

$$\dot{\hat{x}}(t) + \hat{x}(t) = F(z(t));$$

$\hat{x}(t)$ synchronizes with the chaotic $x(t)$, and therefore, $\hat{s}(t) = z(t) - \hat{x}(t-\tau) = s(t)$.

The advantage of this approach is that it allows to recover encoded message ideally (at least if there is no distortion in the channel). An example demonstrating experimental evidence of synchronization in time-delayed systems are recent studies of ring-laser systems [11, 17]. In these experiments, the dynamics of one laser was affected by binary digital information, which was then retrieved from the second nonlinear laser amplifier through use of a suitable detection scheme.

The type of coupling described above is of particular interest for us since it allows to combine nonlinear systems with delayed feedback(s) into a chaotic communication system. There are several properties of nonlinear feedback loops that make them attractive for use in private communications. One is that the dynamics of some common sources of signals in well-known communication systems may be chaotic, and their dynamics is often described by nonlinear delayed differential equations (DDEs). Examples of such systems are a ring laser, and

a traveling wave tube (TWT) amplifier [15, 16] which is widely used in communication satellites. Despite their simplicity, many nonlinear feedback loops are known to exhibit very complex high-dimensional chaotic dynamics which makes them attractive from the security point of view. Another attractive property of chaotic systems is their ability to self-synchronize, obviating the need for precise clock synchronization of communicating agents.

3.2.2   Experimental Setup

We now describe a simple experiment which demonstrates a practical application of nonlinear feedback loops for private communication use. We use a pair of electronic circuits which are an electronic representation of the Mackey-Glass system which is described by the following delayed-differential equation:

$$\alpha \dot{x} + x = \beta \frac{x(t-\tau)}{1 + x(t-\tau)^{10}}.$$

This system is chaotic for sufficiently large values of ratio of τ to α. Also, the dimension of the dynamics grows almost linearly with $\frac{\tau}{\alpha}$ and exceeds 10 for $\frac{\tau}{\alpha} > 10$ A circuit implementation of the Makey-Glass equation is described in detail in [12]. The simplicity of this dynamical system along with its complex behavior makes it a good candidate for experimental trial.

In the following we comment on the schematic of the whole communication setup (see Fig.3.11). The nonlinear element is realized using a complementary pair of JFET transistors coupled in a special way; the experimental plot of the I-V curve of such a nonlinearity loaded with 470 Ohm resistor is shown in Fig.3.12. One can see that for small input voltages, the output current grows almost linearly, whereas for large amplitudes, the gain quickly goes to zero. Such a nonlinearity mimics analytical function $\text{const}\frac{x}{1+x^{10}}$. As a consequence, we will see that

the qualitative behavior of both the numerically integrated Mackey-Glass system and the modeling electronic circuit are very much alike. To implement the delay we use an LC network consisting of 25 resonant sections with a total delay time of 180 μs. We test the delay by measuring its gain as a function of frequency (Fig.3.13) and observe that its fairly constant up to approximately 20 kHz.

Fig.3.14 shows a single pulse after it has propagated through the delay line. We choose characteristic times of the system such that the peak of average power density of the chaotic signal effectively covers the voice signal range (about 2kHz). This choice provides us with superior masking of an information bearing audio signal. The characteristic time α is chosen to be 25 μs which corresponds to $\frac{\tau}{\alpha} = 6.6$. As the voice signal is extracted in the receiver, it is filtered with a low-pass filter to reduce a chaotic residual component which is always present due to non-ideal matching of electronic components. We use second order Chebyshev filter with a 3 kHz cutoff point.

To extend this idea we mention that success of such an experiment would very much rely on the ability to have well matched elements in the receiver and transmitter. The biggest problem comes from JFET nonlinearity since it is described by continuous functions (not by just a finite set of parameters) and those are hard to match. Differences in nonlinearities originate from large deviations in unit-to-unit transistor characteristics, and are worsened after transistors are coupled in pairs. To reduce this effect, we vary a load of one of the nonlinearities and control the linear gain at the same time until we achieve the best possible match.

A convenient way to input a message is to use the op-amp U3 as an adder. It is important to remember that unlike in the Mackey-Glass equation, the nonlin-

earity Q1Q2 in the circuit is not symmetric about zero and it only has a desired I-V characteristic for positive voltages. Therefore, an input message must have the same sign as a chaotic signal at the input of U3. Varying the value of resistor R4 we control the strength of coupling of input signal with the state variable x. For further references, let us call A a signal at the input of U3 and B a signal at the end of the delay line.

To test our circuits for masking voice messages, we use a "Walkman" as a source of information. The attenuated output of our "Walkman" is fed into point A of the transmitter. Attenuation is necessary to keep the perturbation caused by voice below the threshold for destroying chaotic oscillations. It is important to remember that chaotic nature of the signal is crucial for both masking and decoding of messages. Then, the output of U3 (inverted $x(t - \tau) - s(t)$) is sent through the channel (this is an ideal wired connection in our case) to the nonlinearity Q3Q4 at the input of the receiver. In the receiver, the estimate $\hat{x}(t - \tau)$ of the $x(t - \tau)$ is obtained and then it is subtracted from the received signal $x(t - \tau) - s(t)$. The decoded voice message $\hat{s}(t)$ is then filtered with the low-pass filter to reduce the chaotic residue.

Fig.3.15 shows the original voice waveform (a), the reconstructed voice waveform (b); also, shown in (c) and (d) are the masked and decoded mesages. One can see that recovered message closely resembles the original one, and that there is no evident correlation between the received and decoded messages (good for privacy!). It is not possible to recognize the encoded message in the transmitted signal, while the recovered message is of good quality.

3.2.3 Conclusion

In this work we demonstrated the possibility of voice signal encoding and recovery using simple electronic time-delayed nonlinear feedback circuits. The distinctive characteristic of Mackey-Glass system is an ability to exhibit a wide spectrum of dynamical behaviors, such as periodic and quasi-periodic oscillations, and chaos which can be high dimentional.

Using the circuits described above, one can perform a variety of experiments, such as voice masking, and study synchronization as well as generalized synchronization, for an array of chaotic time-delay loops coupled in various ways.
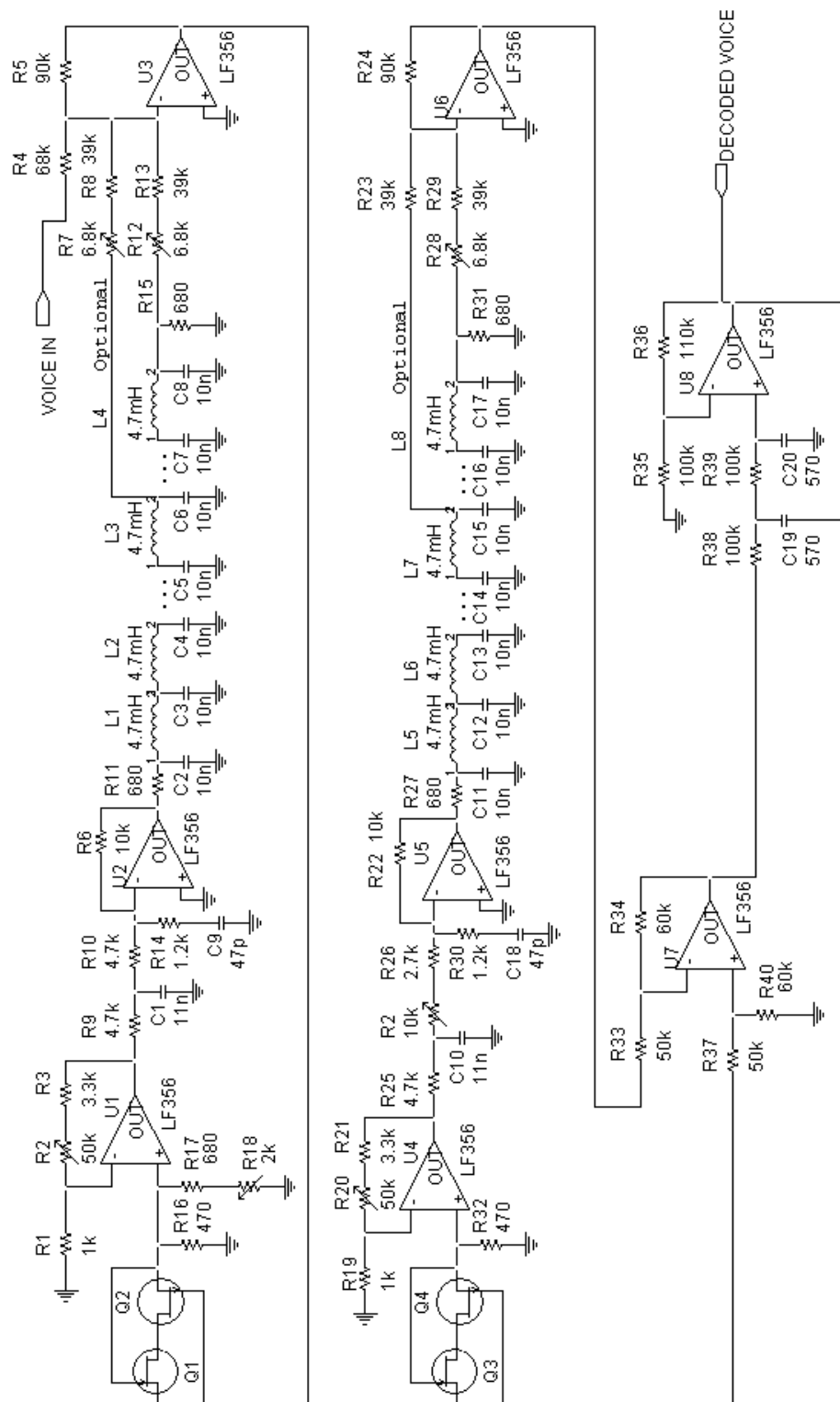
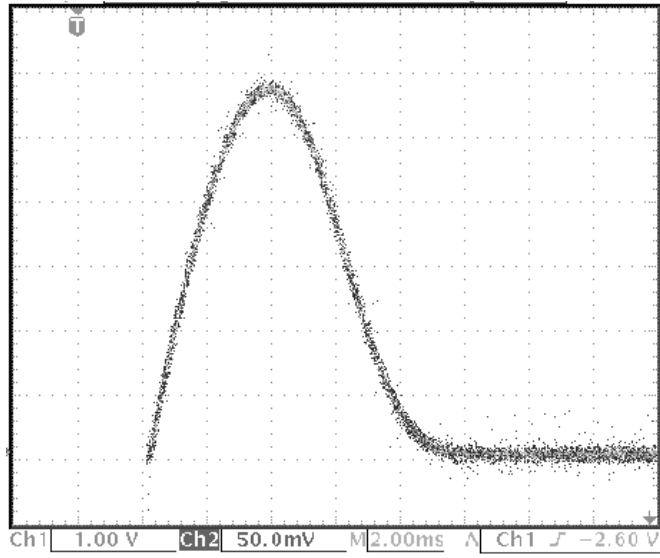Figure 3.11: Schematic diagram of our experimental setup.
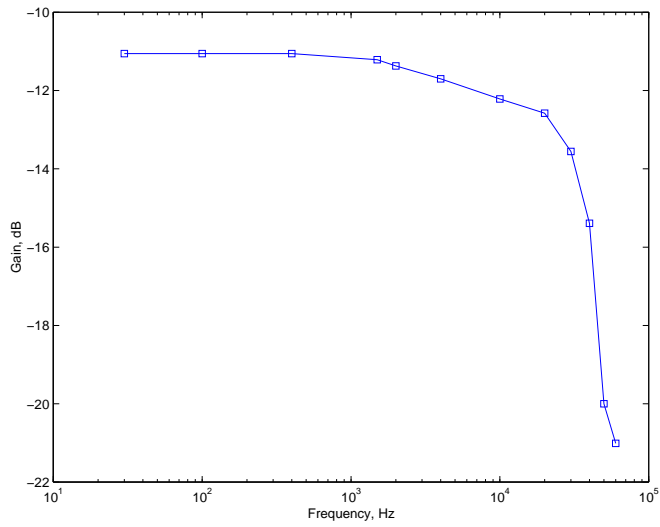
Figure 3.12: Transistor-based nonlinearity.

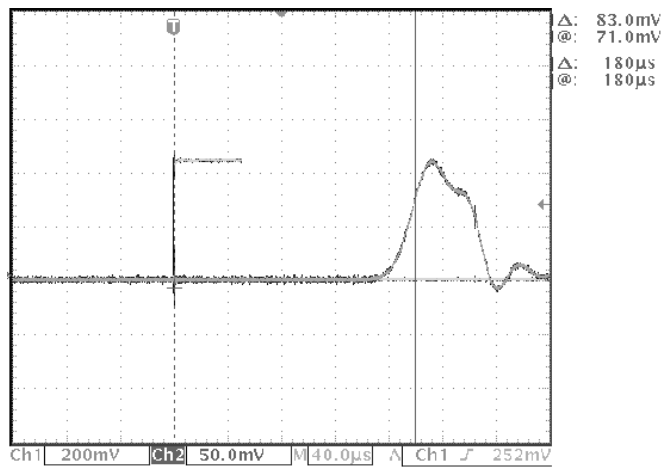Figure 3.13: Delay line characteristic: gain as a function of frequency.
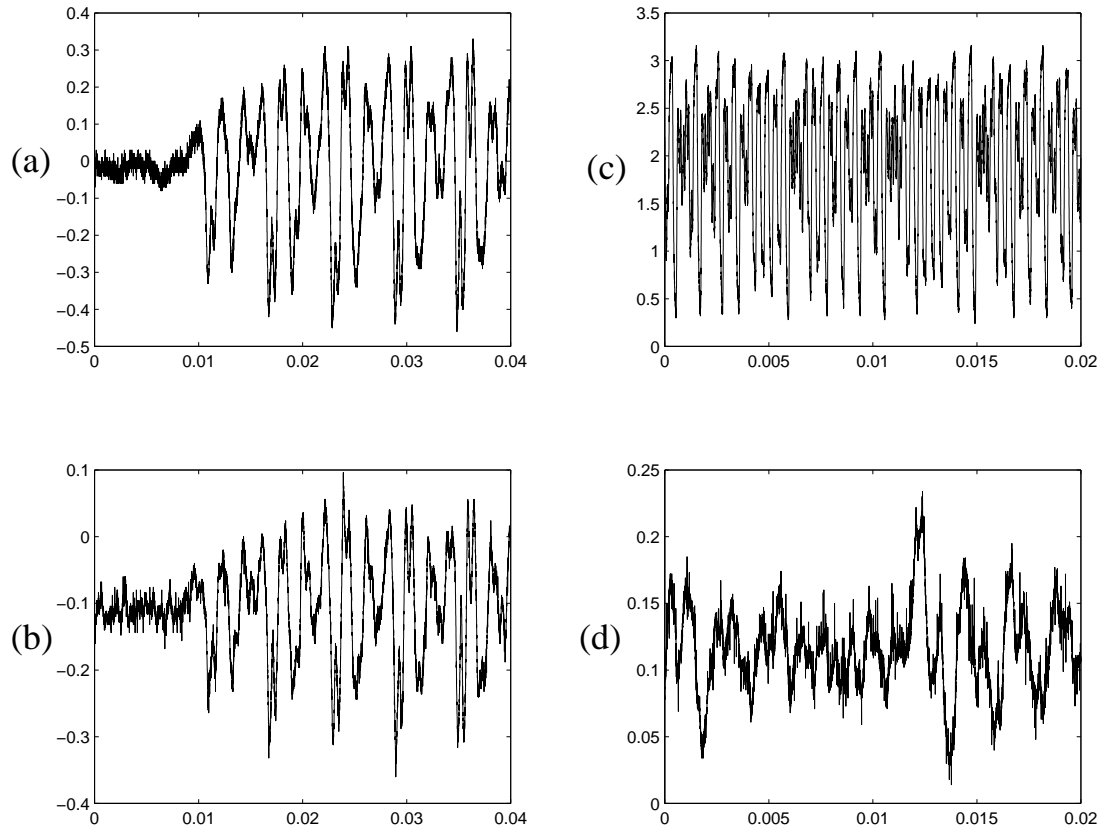
Figure 3.14: Impulse response of the delay line.

Figure 3.15: Original voice signal (a), reconstructed voice signal (b); also, masked and decoded mesages are shown in (c,d). Signal in (a) was measured at VOICE IN port of the circuit, (see Fig.3.11) signals in (b) and (d) were measured at port DECODED VOICE, and (c) was measured at the output of U3.

BIBLIOGRAPHY

[1] V.S. Afraimovich, N.N. Verichev, and M.I. Rabinovich, Stochastic Synchronization of Oscillation in Dissipative Systems, *Radiophys. Quantum Electron.* **29**, 795-803 (1986).

[2] L. Pecora, and T. Carroll, Synchronization in Chaotic Systems, *Phys. Rev. Lett.* **64**, 821 (1990).

[3] J. C. Alexander, I. Kan, J. A. Yorke and Z. You, Int. J. Bif. and Chaos **2**, 795 (1992).

[4] J. C. Sommerer and E. Ott, Nature **365** 136 (1993).

[5] C. Castillo-Chavez and A.- A. Yakubu, Intraspecific competition in discrete-time patchy environments. Ithaca : Cornell University 2000.

[6] A. H. W. Beck, *Velocity-Modulated Thermionic Tubes* [Cambridge University Press, 1948]

[7] J. F. Gittins, *Power Travelling-Wave Tubes* [New York, American Elsevier Pub. Co., 1965]

[8] J. R. Pierce, *Traveling Wave Tubes* [Prinston, NJ: Nostrand, 1950]

[9] M.C. Makey and L. Glass, Oscillation and Chaos in Physiological Control System, *Science* **197** (1977) 287.

[10] V. Udaltsov, J. Goedgebuer, L. Larger, and W. Rhodes, Dynamics of Non-linear Feedback Systems with Short Time-Delays

[11] G. Vanwiggeren and R. Roy, Chaotic Communication Using Time-Delayed Optical Systems, *Int. J. of Bifurcation and Chaos*, **9**, No 11 (1999) 2129.

[12] A. Namajunas, K. Pyragas, A. Tamasevicius, An Electronic Analog of the Mackey-Glass system,*Physics Letters A* **201** (1995), 42

[13] A. Namajunas, K. Pyragas, A. Tamasevicius, Stabilization of an Unstable Steady-State in a Mackey-Glass System, *Physics Letters A* **204** (1995), 255

[14] T. Aida, P. Davis, Oscillation Modes of Laser Diode Pumped Hybrid Bistable System with Large Delay and Application to dynamical Memory, *IEEE J. of Quantum Electronics*, Vol 28, No.3. (1992) 690

[15] V. Dronov, M. Hendrey, T. Antonsen, and E. Ott, Communicating with Chaos Using a Traveling Wave Tube Microwave Generator, *Chaos* 14, 30 (2004).

[16] P. N. Safier, V. Dronov, T. M. Antonsen Jr., J. Qiu, B. G. Danly, and B. Levush, *From Frequency-Domain, Physics-Based Modeling to Time-Domain Simulation of High Data-Rate Performance*, (presented at 2001 MTT Conference).

[17] H. Abarbanel and M. Kennel, Synchronizing High-Dimensional Chaotic Optical Ring Dynamics, *Phys. Rev. Lett.* **80** No.14 (1998), 3153

[18] A. A. M Saleh, *Frequency-Independent and Frequency-Dependent Nonlinear Models of TWT Amplifier* [IEEE Transactions on Communications, vol. COM-29, no. 11 pp. 1715-1720, November, 1981]

[19] M. C. Jeruchim, P. Balaban and K. S. Shanmugan, *Simulation of Communication Systems*, [New York: Plenum Press, 1992]

[20] T. M. Antonsen Jr. and B. Levush, *CHRISTINE: A multifrequency parametric simulation code for traveling-wave tube amplifiers* [NRL Rep. 97-9845, 1997]

[21] David K. Abe, Mai T. Ngô, Baruch Levush, T. M. Antonsen Jr. and David P. Chernin, *A comparison of L-Band Helix TWT Experiments with CHRISTINE, a 1-D Multifrequency Helix TWT Code* [IEEE Transactions on Plasma Science, Vol. 28, No. 3, June 2000]

[22] John G. Wöhlbier, John H. Booske, and Ian Dobson *New Nonlinear Multifrequency TWT model* [2nd IEEE International Vacuum Electronics Conference, Huis ter Duin, Noordwijk, Netherlands, April 02-04, 2001]

[23] E. Ott, *Chaos in Dynamical Systems* [Cambridge University Press, 1993], Chapter 4

[24] E. Bolt and M. Dolnik, Encoding Information in Chemical Chaos by Controlling Symbolic Dynamics,*Phys Rev E*, **55**, No.6 (1997) 6404.

[25] S. Hayes, C. Grebogi, and E. Ott, Communicating with Chaos, *Phys. Rev. Lett.* **70**, 3031 (1993).

[26] S. Hayes, C. Grebogi, E. Ott, and A. Mark, Experimental Control of Chaos for Communications, *Phys. Rev. Lett.* **73**, 1781 (1994).

[27] E. Ott, C. Grebogi, and J. Yorke, Controlling Chaos, *Phys. Rev. Lett.* **64**, 1196 (1990).

[28] V. S. Udaltsov, J. Goedgebuer, L. Larger, and E. T. Rhodes, Communicating with Synchronized Hyperchaos.

[29] A. R. Volkovskii and L. S. Tsimring, Synchronization and Communication Using Chaotic Frequency Modulation., 1999

[30] N. F. Rulkov, M. M. Suschik, L. S. Tsimring, A. R. Volkovskii, H. Abrbanel, L. Larson, and K. Yao, Digital Communication Using Chaotic Pulse Generators.

[31] K. Cuomo, and A. Oppenheim, Circuit Implementation of Synchronized Chaos with Applications to Communications, *Phys. Rev. Lett.* **71**, 66 (1993).

[32] L. Kocarev and U. Parlitz, General Approach for Chaotic Communication with Applications to Communication, *Phys. Rev. Lett.* **74**, 5028 (1995).

[33] L. Tsimring, M. Sushchik, Multiplexing Chaotic Signals using Synchronization, *Physics Letters A* **213** (1996), 155

[34] H. Torikai and Toshimichi Saito,A Multiplex Communication System Using Chaotic Pulse-Trains with Sawtooth Control, IEEE International Symposium on Circuits and Systems, June 9-12, 1997, Hong-Kong

[35] J. Milnor, Commun. Math. Phys. **99**, 177 (1985).

[36] E. Ott, J. C. Alexander, I. Kan, J. C. Sommerer, and J. A. Yorke, Physica D **76**, 384 (1994); Phys. Rev. Lett. **71**, 4134 (1993).

[37] P. Ashwin, J. Buescu, and I. N. Stewart, Phys. Lett. A **193**, 126 (1994); Nonlinearity **9**, 703 (1996).

[38] P. Ashwin, E. Covas and R. Tavakol, Nonlinearity **12**, 563 (1999).

[39] S. C. Venkataramani, B. Hunt, and E. Ott, Phys. Rev. E **54**, 1346 (1996).

[40] Diffusion models have also been used in the related problem of on-off inter-

mittency. For example, see T. Yamada and H. Fujisaka, Prog. Theor. Phys. **76**, 582 (1986); H. Hata and S. Miyazaki Phys. Rev. E **55**, 5311 (1997).

[41] S. W. McDonald, C. Grebogi, E. Ott and J. A. Yorke, Physica D **17**, 125 (1985).

[42] Y. Pomeau and P. Manneville, Commun. Math. Phys. **74**, 189 (1985).

[43] W. Yang, M. Ding, A. J. Mandell, and E. Ott, Phys. Rev. E **51**, 102 (1995).

[44] Y. C. Lai and C. Grebogi, Phys. Rev. Lett. **83**, 2926 (1999).

[45] S. Haykin, *Communication Systems* [John Wiley & Sons, Inc., 1994]

[46] We have also obtained preliminary results of numerical modeling for a second order model in which the linear part of the TWT is modeled with a second order maximally flat filter (which would be a more precise description of a real TWT). With the second order filter, Eq.(3.2) is modified by the addition of a term $d^2A(t)/dt^2$ and changing $dA(t)/dt$ to $\sqrt{2}dA(t)/dt$ on the left-hand side. For a certain set of model parameters we observe again a low-dimentional chaotic flow (Fig.3.9) which can be controlled using the technique described above for a first-order model. Now, however, the phase of the signal changes more sporadically. This results in a much smaller carrier power (11% of total signal power as compared to 70% for the first order model) and, therefore, higher power efficiency.